Int J Earth Sci (Geol Rundsch) (2006) 95: 318–340
DOI 10.1007/s00531-005-0025-y

ORIGINAL PAPER

Nikolay Bonev · Jean-Pierre Burg · Zivko Ivanov

Mesozoic–Tertiary structural evolution of an extensional gneiss dome—the Kesebir–Kardamos dome, eastern Rhodope (Bulgaria–Greece)

Received: 25 April 2003 / Accepted: 18 June 2005 / Published online: 25 August 2005

Abstract The tectonic evolution of the Rhodope massif involves Mid-Cretaceous contractional deformation and protracted Oligocene and Miocene extension. We present structural, kinematic and strain data on the Kesebir–Kardamos dome in eastern Rhodope, which document early Tertiary extension. The dome consists of three superposed crustal units bounded by a low-angle NNE-dipping detachment on its northern flank in Bulgaria. The detachment separates footwall gneiss and migmatite in a lower unit from intermediate metamorphic and overlying upper sedimentary units in the hanging wall. The high-grade metamorphic rocks of the footwall have recorded isothermal decompression. Direct juxtaposition of the sedimentary unit onto footwall rocks is due to local extensional omission of the intermediate unit. Structural analysis and deformational/metamorphic relationships give evidence for several events. The earliest event corresponds to top-to-the SSE ductile shearing within the intermediate unit, interpreted as reflecting Mid-Late Cretaceous crustal thickening and nappe stacking. Late Cretaceous–Palaeocene/Eocene late-tectonic to post-tectonic granitoids that intruded into the intermediate unit between 70 and 53 Ma constrain at least pre-latest Late Cretaceous age for the crustal-stacking event. Subsequent extension-related deformation caused pervasive mylonitisation of the footwall, with top-to-the NNE ductile, then brittle shear. Ductile flow was dominated by non-coaxial deformation, indicated by quartz *c*-axis fabrics, but was nearly coaxial in the dome core. Latest events relate to brittle faulting that accommodated extension at shallow crustal levels on high-angle normal faults and additional movement along strike-slip faults. Radiometric and stratigraphic constraints bracket the ductile, then brittle, extensional events at the Kesebir–Kardamos dome between 55 and 35 Ma. Extension began in Paleocene–early Eocene time and displacement on the detachment led to unroofing of the intermediate unit, which supplied material for the syn-detachment deposits in supra-detachment basin. Subsequent cooling and exhumation of the footwall unit from beneath the detachment occurred between 42 and 37 Ma as indicated by mica cooling ages in footwall rocks, and extension proceeded at brittle levels with high-angle faulting constrained at 35 Ma by the age of hydrothermal adularia crystallized in open spaces created along the faults. This was followed by Late Eocene–Oligocene post-detachment overlap successions and volcanic activity. Crustal extension described herein is contemporaneous with the closure of the Vardar Ocean to the southwest. It has accommodated an earlier hinterland-directed unroofing of the Rhodope nappe complex, and may be pre-cursor of, and/or make a transition to the Aegean back-arc extension that further contributed to its exhumation during the Late Miocene. This study underlines the importance of crustal extension at the scale of the Rhodope massif, in particular, in the eastern Rhodope region, as it recognizes an early Tertiary extension that should be considered in future tectonic models of the Rhodope and north Aegean regions.

Keywords Gneiss dome · Ductile strain · Detachment fault · Crustal extension · Rhodope

N. Bonev (✉)
Faculty of Geosciences and Environment,
Institute of Geology and Paleontology, University of Lausanne,
BFSH 2, 1015 Lausanne, Switzerland
E-mail: nikolay.bonev@unil.ch
Tel.: +41-21-6924359
Fax: +41-021-6924305

J.-P. Burg
Geologisches Institut, ETH Zentrum and University Zürich,
Sonnegstrasse 5, 8092 Zurich, Switzerland

Z. Ivanov · N. Bonev
Department of Geology and Paleontology,
Faculty of Geology and Geography,
Sofia University "St. Kliment Ohridski",
15 Tzar Osvoboditel Bd, 1504 Sofia, Bulgaria

Introduction

Collisional orogens have often experienced syn-thickening to post-thickening extensional deformation (e.g.

Coney and Harms 1984; Platt 1986; Dewey 1988; Ratschbacher et al. 1989; Burg et al. 1994). Gneiss domes bounded by low-angle detachment faults are typically related to orogenic extension (e.g., Brun 1983; Selverstone 1988; Teyssier and Whitney 2002) and the detachment faults play an effective role in exhuming high-grade footwall rocks (e.g. Davis et al. 1980; Wernicke 1981; Wernicke and Burchfiel 1982; Hodges et al. 1987).

A protracted extensional history in the north Aegean region and the Rhodope massif (inset, Fig. 1) since at least the Late Cretaceous until the Late Neogene has

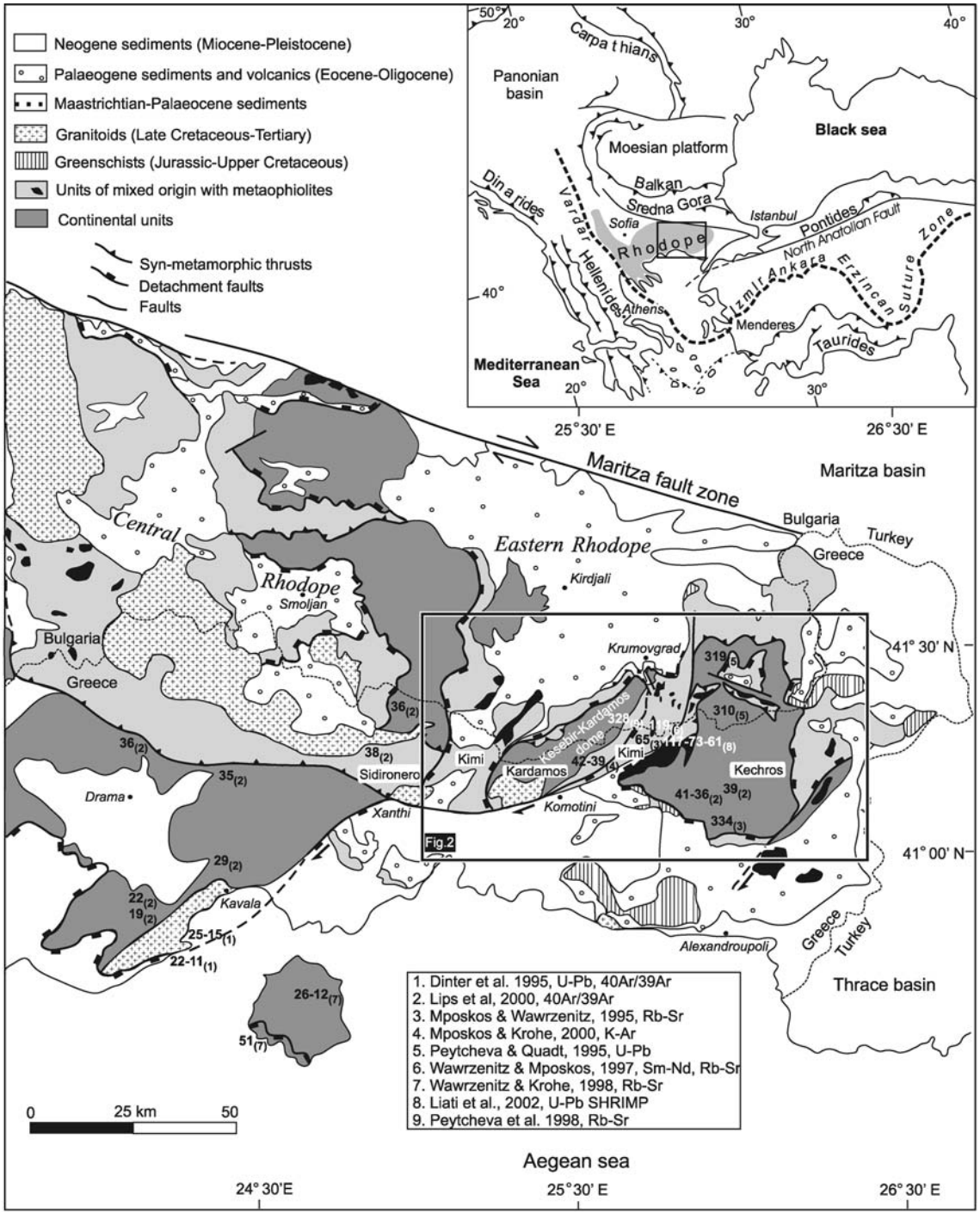

Fig. 1 Synthetic tectonic map of the central and eastern Rhodope in Bulgaria and Greece [modified after Burg et al. (1996); Dinter (1998); Krohe and Mposkos (2002)], showing the main tectonic units referred to in the text with compilation of published geochronologic data (numbers with indices, *numbers* radiometric ages, *indices* bibliographic reference as indicated in frame, in the figure). *Inset* location of the Rhodope Massif in a framework of the Alpine collisional system in the eastern Mediterranean

produced exhumation of mid crustal to lower crustal metamorphic complexes beneath mylonitic extensional shear zones (Lister et al. 1984; Dinter and Royden 1993; Schermer 1993; Sokoutis et al. 1993; Hetzel et al. 1995; Wawrzenitz and Krohe 1998; Bonev 1999, 2002). The Kesebir dome in the eastern Rhodope of Bulgaria will be named hereafter the Kesebir–Kardamos dome to account for the regional correlations with its southwestern extension in Greece (Fig. 2; Krohe and Mposkos 2002). The purposes of this paper are: (1) to document structures and kinematic features related to the Early Tertiary dome-formation; (2) to establish the ductile strain regime; and (3) to use these structures in interpreting the regional tectonic evolution. We conclude that the Kesebir–Kardamos dome results from Late Cretaceous–early Tertiary syn-thickening to post-thickening extension of the Rhodope region, which was pre-cursor to the Miocene Aegean extension (e.g. Dinter and Royden 1993; Sokoutis et al. 1993; Dinter 1998; Gautier et al. 1999).

Regional tectonic setting and geological framework

Tectonic setting

The Rhodope massif is part of the Alpine–Himalayan mountain chains in the eastern Mediterranean (Fig. 1,

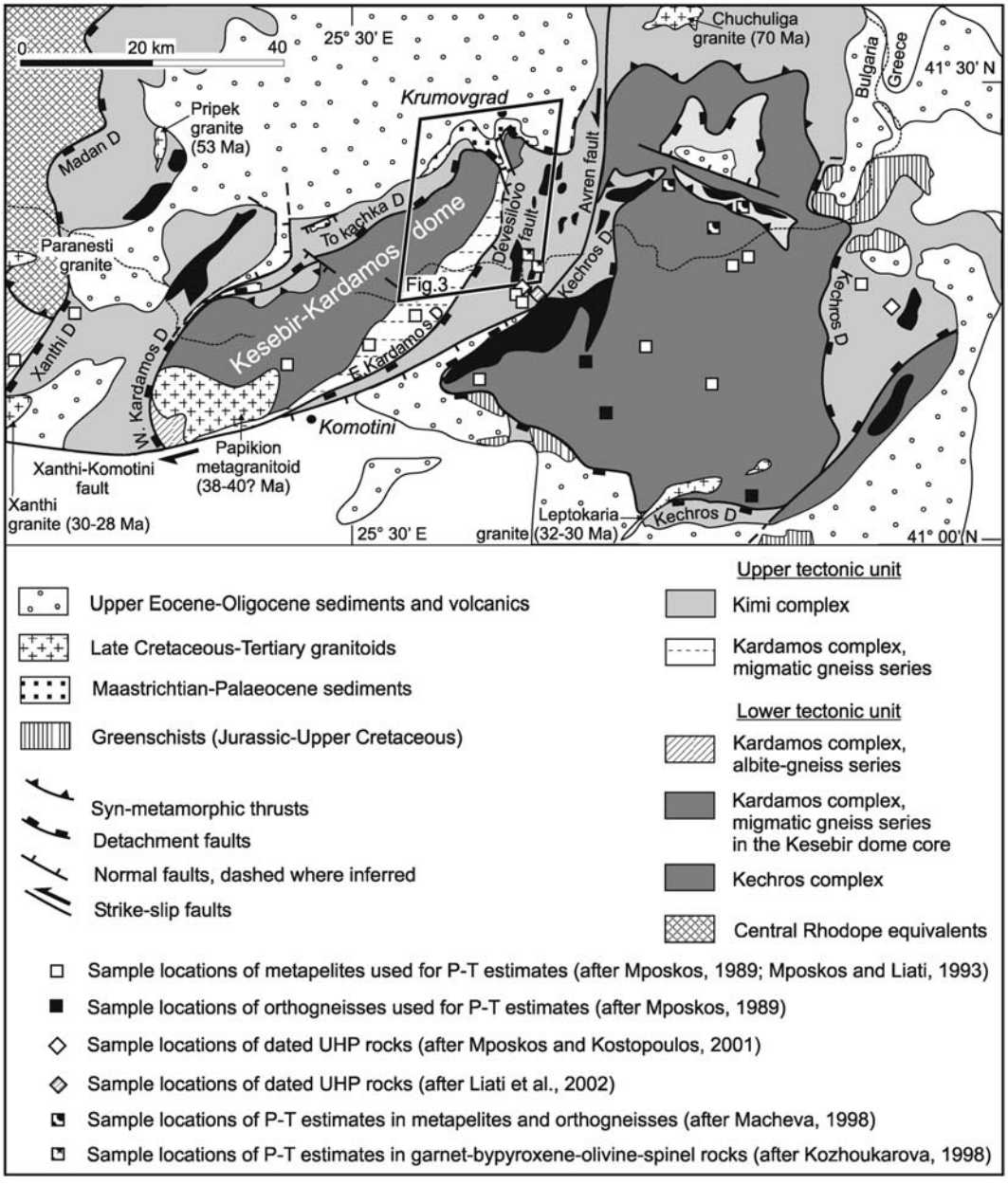

Fig. 2 Tectonic sketch map of the eastern Rhodope showing correlation between units and detachments across the Greece–Bulgaria border. *Squares* sites of P–T estimates referred to in the text and indicated in Fig. 4. See also Fig. 1, and Krohe and Mposkos (2002)

inset). It is separated from the Late Cretaceous Sredna Gora basin, to the north, by the Alpine Maritza dextral strike-slip fault zone. The Rhodope massif is bordered to the northeast and to the east by the Late Paleogene–Neogene Maritza and Thrace basins and, to the west, by intermediate to low-grade rocks of the Vardar suture zone. The southern parts of the Rhodope massif are hidden in the north Aegean Sea. The Rhodope massif is mainly composed of amphibolite facies rocks derived from magmatic and sedimentary protoliths, locally enclosing eclogites (Liati 1988; Liati and Mposkos 1990) and intruded by Late Cretaceous to Mid-Tertiary plutonic rocks (Jaranov 1960; Meyer 1968, 1969; Kronberg and Raith 1977; Soldatos and Christofides 1986; Dinter et al. 1995; Peytcheva et al. 1999). Voluminous Oligocene felsic and basic volcanic rocks (Harkovska et al. 1989; Yanev and Bardintzeff 1997) and Late Cretaceous/Early Tertiary to Pliocene sediments (Goranov and Atanasov 1992; Boyanov and Goranov 2001) cover the crystalline rocks.

The mountain belt of the southeastern Balkan Peninsula reflects Mesozoic–early Cenozoic subduction and collision in the Tethys realm (Dewey and Sengör 1979; Dercourt and Ricou 1987; Ricou 1994; Robertson et al. 1996). The Rhodope massif results from Late Cretaceous to early Tertiary convergence and collision of the continental promontory with Adriatic–Apulian affinity in the south with the Moesian platform (Eurasia) to the north (e.g. Robertson and Dixon 1984; Dercourt et al. 1986). Radiometric dates from the northernmost Aegean domain record active convergence in Mid-Cretaceous times (e.g. Schermer 1993; Lips et al. 1998). The Rhodope massif was formed as a metamorphic wedge paired with the Vardar olistostromic trench (Ricou et al. 1998). Crustal shortening and thickening in the convergent region involved both coeval and subsequent extension (Burg et al. 1996).

Geological framework

The central and eastern Rhodope in Bulgaria and Greece (Fig. 1) comprises several, flat-lying tectono–metamorphic complexes separated by tectonic contacts. Recent syntheses divide the metamorphic pile into a lower and an upper terrane sandwiching intermediate thrust sheets (Burg et al. 1996). Geochronologic ages generally decrease southwestward.

The eastern Rhodope high-grade metamorphic pile has been initially subdivided into a lower tectonic unit and an upper tectonic unit on general geologic and petrologic grounds (Mposkos 1989; Mposkos and Liati 1993). The recent subdivision into the Kardamos Complex (Mposkos 1998; Mposkos and Krohe 2000) and Kechros Complex (Mposkos and Krohe 2000) as lowermost entities and an overlying Kimi Complex (Mposkos and Krohe 2000) is made on the basis of contrasting metamorphic, geochronologic and structural information (Krohe and Mposkos 2002). The Kardamos Complex is further subdivided into a lower (e.g. albite-gneiss series) and upper (e.g. migmatic gneiss series) series. The simpler subdivision of the eastern Rhodope high-grade metamorphic pile into a lower tectonic unit (including part of Kardamos and Kechros Complexes) and an upper tectonic unit (Kimi Complex) is preferred here, because it reflects coherent lithologies of the footwall and the hanging wall of low-angle detachment systems in both northern Greece and south Bulgaria (Fig. 2), taking into account the radiometric ages, stratigraphic and kinematic information on a regional scale. The upper unit comprises interlayered amphibolites, marbles, metapelitic schists and various gneisses enclosing eclogite and metaophiolite lenses (Ivanov 1988; Burg et al. 1996). In our identification, however, the upper tectonic unit includes the Kimi Complex and also lithologically indistinguishable from the latter the upper part of the Kardamos Complex. The lower tectonic unit is mainly composed of a succession of orthogneiss and migmatitic gneiss with some paragneiss in Bulgaria (Ivanov 1988), to which the overlying succession of alternating pelitic gneisses, amphibolites and marbles in Greece have been assigned (Mposkos 1998; Krohe and Mposkos 2002). It is equivalent to the two structurally lowest complexes defined by Krohe and Mposkos (2002) in Greece, except the upper amphibolite, schist and marble-bearing levels in migmatic gneiss series of the Kardamos Complex on the southern flank of the Kesebir–Kardamos dome, which belong to the upper unit (Fig. 2). In the high-grade metamorphic complex at the latitude of the Kesebir–Kardamos dome, the upper tectonic unit occupies intermediate position occurring below the structurally upper sedimentary unit of cover sequences. Therefore, the designation ''intermediate unit'' in the following litho-tectonic subdivision and description refers to the upper tectonic unit of regional-scale subdivision of the high-grade metamorphic complex.

Metamorphism

Three metamorphic events are identified mostly by previous workers in Greece, and in Bulgaria as well—high-pressure eclogite facies, medium-pressure amphibolite facies and late greenschist facies metamorphism (Liati 1986; Mposkos 1989; Mposkos and Liati 1993; Wawrzenitz and Krohe 1998). Diamond and coesite inclusions in garnet indicate earliest ultrahigh-pressure conditions >26 kbar and above 900°C in the Sideronero Complex of central Rhodope and the Kimi Complex in the eastern Rhodope (Mposkos and Kostopoulos 2001). The high-pressure/high-temperature eclogite/granulite facies conditions in the Kimi Complex of the upper unit ($P\sim13.5$–16 kbar; $T\sim750$–775°C) decreased to ca. 10 kbar and 600–650°C in the medium-pressure event, subsequently retrogressed into the greenschist facies (Mposkos and Krohe 2000). Similarly, in the same unit, eclogite facies conditions ($P\sim12$–17 kbar; $T\sim750$–

811°C) decreased to P∼8–10 kbar and T∼560–623–C during the medium-pressure event (Kozhoukharova 1998). The lower unit, in the case Kardamos Complex, records nearly isothermal decompression from maximum pressures of 13–16 kbar for an assumed temperature of 600°C (including some eclogites, Mposkos and Liati 1993), followed by amphibolite facies overprint at pressure <8 kbar and temperatures of 560–620°C (Mposkos 1998). In Bulgaria, the high-pressure event at P∼13 kbar and T∼450°C was followed by medium-pressure amphibolite-facies conditions (P∼9–3 kbar; T∼550°C) and low-pressure/low-temperature retrogressive stage (P∼3–2 kbar; T∼400°C) (Macheva 1998).

Summarizing, the metamorphic record indicates peak conditions of ultrahigh/high-pressure metamorphism in the upper levels of the tectono-stratigraphic pile, and lower pressures in eclogite facies rocks of the underlying complexes.

Geochronologic data

Geochronologic studies on metamorphic complexes of the central and eastern Rhodope are compiled in Table 1, and ages relevant to this study are shown in Figs. 1 and 3.

Lower unit protolith ages obtained by U–Pb zircon dating of rocks equivalent to the Kechros Complex orthogneisses range between 319 and 305 Ma (Peytcheva and Quadt 1995), which gives support to the 334 Ma Rb–Sr isochron age of a metapegmatite in the latter (Mposkos and Wawrzenitz 1995) and the 328 Ma Rb–Sr whole-rock data of an orthogneiss (Peytcheva et al. 1998) in the core of the Kesebir–Kardamos dome. The age of the high-pressure metamorphism is specified by the 119 Ma Sm–Nd isochron from a garnet pyroxenite (Wawrzenitz and Mposkos 1997) although a similar, 117 Ma U–Pb SHRIMP age of zircon domains in another garnet pyroxenite is interpreted as a protolith age (Liati et al. 2002). The U–Pb technique yielded an age of 73 Ma for the eclogite-facies metamorphism (Liati et al. 2002), and an age of 62 Ma for the retrograde stage. The latter age is consistent with the 65 Ma Rb–Sr muscovite age from a pegmatite (Mposkos and Wawrzenitz 1995). Wawrzenitz and Krohe (1998) dated medium-pressure metamorphism between 51 and 39 Ma. In contrast to the above metamorphic ages, and in contradiction with the sedimentary cover constraints, Liati and Gebauer (1999) suggested that the high-, medium- and low-pressure events took place between 45 and 36 Ma.

Cooling ages of 42–39 Ma obtained from K–Ar dating on micas distinguish the thermal evolution of the lower unit below 350–300°C (Krohe and Mposkos 2002). Recent $^{40}Ar/^{39}Ar$ biotite and muscovite ages in the Bulgarian part of the dome constrain cooling of the lower unit below 350–300°C at 38–37 Ma (Marchev et al. 2003). Supportively, $^{40}Ar/^{39}Ar$ data on micas from central and eastern Rhodope indicate Middle–Late Eocene cooling below 350°C between 41 and36 Ma (Dinter 1998; Lips et al. 2000), followed by cooling to 150–

Table 1 Summary of geochronologic data

Method	Minerals	Age (Ma)	Unit/Sample	References
K–Ar	Ms	42.1 ± 1	Kardamos/orthogneiss	Krohe and Mposkos (2002)
	Bt	39.4 ± 1	Kardamos/orthogneiss	§
40Ar/39Ar	Ms	42.37 ± 2.30	Kechros/augen gneiss	Lips et al. (2000)
	Ms	39.27 ± 5.38	Kechros/mylonite	§
	Ms	36.15 ± 1.10	Sidironero/quartz vein	§
	Ms	39.71 ± 2.97	Sidironero/contact marble	§
	Ms	36.14 ± 4.99	Pangeon/gneiss	§
	Ms	35.68 ± 6.08	Pangeon/mylonite	§
	Ms	38.13 ± 0.36	Kesebir/muscovite gneiss	Marchev et al. (2003)
	Bt	37.73 ± 0.25	Kesebir/augen gneiss	§
	Adularia	34.99 ± 0.23	Kesebir/Qtz-Adularia alteration	§
Rb–Sr	Ms	334.6 ± 3.4	Kechros/metapegmatite	Mposkos and Wawrzenitz (1995)
	w. r.	328 ± 25	Kesebir/metagranite	Peytcheva et al. (1998)
	Ms	65.4 ± 0.7	Kimi/pegmatite	Mposkos and Wawrzenitz (1995)
	Ms	51.4 ± 0.8	Thasos/pegmatoid	Wawrzenitz and Krohe (1998)
	Bt	40.3 ± 0.4	Thasos/gneiss	§
	Bt	39.0 ± 0.4	Thasos/gneiss	§
Sm–Nd	Grt-Cpx	119.6 ± 3.5	Kimi/pyroxenite	Wawrzenitz and Mposkos (1997)
U–Pb	Zr	319 ± 9–310 ± 5.5	Biala reka/metagranite	Peytcheva and Quadt 1995)
	Zr-Mnz	52.89 ± 0.89	Pripek granite	Ovtcharova et al. (2003)
	Zr	70	Chuchuliga granite	Marchev et al. (2004a)
U–Pb SHRIMP	Zr	117.4 ± 1.9	Kimi/pyroxenite	Liati et al. (2002)
	Zr	73.5 ± 3.5	Kimi/pyroxenite	§
	Zr	61.9 ± 1.9	Kimi/pegmatite	§
	Zr	45.3 ± 0.9	Sidironero/quartz vein	Liati and Gebauer (1999)
	Zr	42.2 ± 0.9	Sidironero/orthogneiss	§
	Zr	36.01 ± 1.2	Sidironero/pegmatite	§

Mineral abbreviations: *Grt* garnet, *Cpx* clinopyroxene, *Bt* biotite, *Ms* muscovite, *Qtz* quartz, *Zr* zircon, *Mnz* monazite, *w. r.* whole rock

300°C and exhumation at 23–12 Ma (Dinter et al. 1995; Wawrzenitz and Krohe 1998; Lips et al. 2000). Late-tectonic to post-tectonic plutons (e.g. Xanthi, Leptokaria and Simvolon) intruded the metamorphic units between 32 and 23 Ma (Liati 1986; Del Moro et al. 1988; Dinter et al. 1995). However, recent radiometric dates of granitoids that have intruded the upper unit in the eastern Bulgarian Rhodope (see Fig. 2, Table 1) yield 70 Ma U–Pb zircon age for the Chuchuliga granite (Marchev et al. 2004a; P. Marchev personal communication 2003) and U–Pb zircon and monazite age of 53 Ma for the Pripek granite (Ovtcharova et al. 2003) providing evidence for at least a pre-latest Late Cretaceous age for the main tectono-metamorphic event in amphibolite-facies.

In summary, the overall metamorphic history of the central/eastern Rhodope took place during Mesozoic convergence and crustal thickening. Geochronological data indicate that crustal material including late Paleozoic granitoids were involved in the tectono-metamorphic process, whereas distinct units probably suffered high-pressure metamorphism at different times. They also show a southward and downward younging direction of cooling ages (Fig. 1).

The Kesebir–Kardamos dome

Overview

The Kesebir–Kardamos dome is a subelliptical metamorphic culmination that trends NE–SW (Figs. 2, 3). The dome is cored by medium-pressure amphibolite facies migmatites and orthogneisses with granitic to granodioritic compositions (Kozhoukharov 1987; Mposkos and Liati 1993). The core is mantled by a

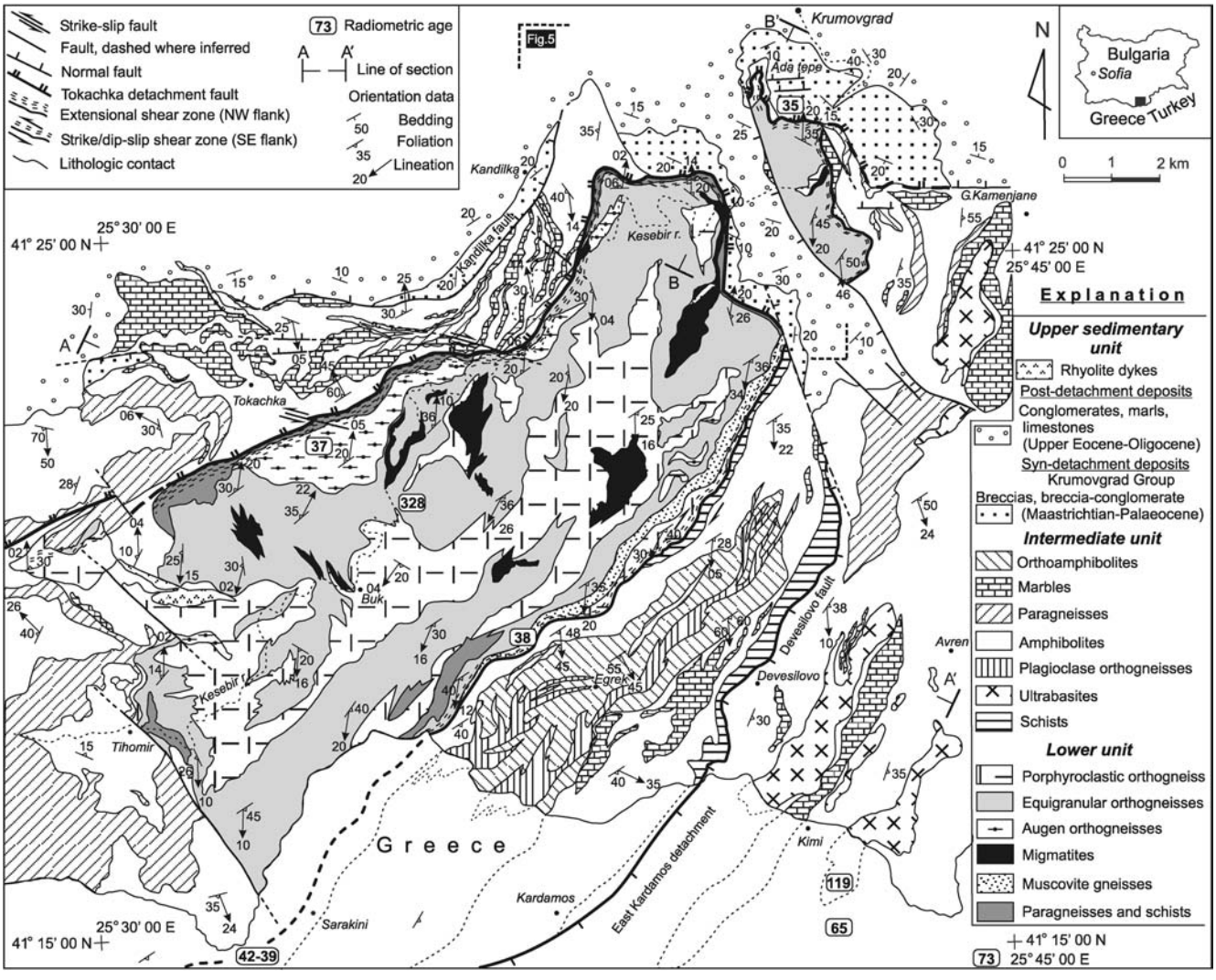

Fig. 3 Simplified geological map of the Kesebir–Kardamos gneiss dome (after Bonev 2002), with location of geochronologic data. See Fig. 1 and Table 1 for references. Extensions of lithologic (*dashed*) and tectonic contacts in Greece are adapted from von Braun (1993) and Krohe and Mposkos (2002). A–A' and B–B' sections of Fig. 6

metamorphic complex consisting of para-derived and ortho-derived rocks with eclogite boudins and lenses of metaophiolites, the latter separated in the hanging wall of the Tokachka detachment fault (Bonev 1996) that bounds mantle from the core on the northern flank of the Kesebir–Kardamos dome.

The main litho-tectonic units and structural elements of the Kesebir–Kardamos dome are, down section: (1) Oligocene volcanic rocks and unmetamorphosed Maastrichtian–Palaeocene to Lower Eocene and Upper Eocene–Oligocene sediments, referred to as upper sedimentary unit; these sediments lay transgressively or tectonically on both metamorphic units on the northern flank of the dome; (2) a structurally intermediate, variegated metamorphic complex, is equivalent to the uppermost levels of the Kardamos Complex and the whole Kimi Complex (Krohe and Mposkos 2002) and corresponds to the upper tectonic unit of the high-grade metamorphic complex; (3) the major low-angle detachment fault zone (the Tokachka detachment fault of Bonev 1996) on the northern flank of the dome, which is unrelated to the eastern Kardamos detachment of Krohe and Mposkos (2002) and its extension Devesilovo fault that cut through the variegated metamorphic complex in southeastern flank of the structure; (4) mylonites of normal shear zones that deformed the upper part of the core gneiss–migmatite complex; (5) the gneiss–migmatite complex, which represents the deepest level of exposure and is equivalent to the lower-middle part of the Kardamos Complex (e.g. migmatic gneiss series) corresponding to the lower tectonic unit of the high-grade metamorphic complex. In the northeastern closure of the dome, Maastrichtian–Paleocene sediments are separated from the lowest unit by the detachment fault zone and thin slices of the intermediate unit, whereas in the west-northwestern part of the dome Upper Eocene–Oligocene sediments rest unconformably on the metamorphic rocks of the intermediate unit (e.g. Goranov and Atanasov 1992). The upper sedimentary and intermediate units form together the hanging wall, and the lower unit constitutes the footwall of the detachment fault system (Fig. 3). Structural and lithologic differences between hanging wall and footwall metamorphic units were used to define litho-tectonic units.

Litho-tectonic subdivisions

Lower unit

The lower unit comprises orthogneiss interlayered with migmatite, paragneiss, and metapelite. The orthogneiss bodies are concordant with the metamorphic foliation of enclosing schists and paragneiss. The sequence includes, from bottom to top (Fig. 4) (1) a more than 600-m-thick sill or laccolith of orthogneisses derived from a porphyritic granite that intruded equigranular orthogneisses. Primary intrusive contacts are generally reworked as mylonite zones; (2) up to 750-m-thick unit of two-mica equigranular to banded orthogneisses with lenses of paragneisses, schists, migmatites and migmatitic gneisses; (3) on the northwestern side of the dome, a sheet-like body of augen orthogneiss; (4) a discontinuous envelope of psammitic paragneisses and pelitic schists.

Paragneisses and metapelites display garnet–biotite–kyanite ± staurolite ± muscovite assemblages. The various orthogneisses consist chiefly of roughly equal amounts of oligoclase, K-feldspar, quartz, biotite ± muscovite. Accessories include rutile, apatite and zircon. Partial melting produced sillimanite-bearing migmatites and migmatitic gneisses, and leucogranite veins that intrude the orthogneisses. Metamorphic conditions are estimated at 550–620°C and <8 kbar (Mposkos and Krohe 2000) on the basis of the mineral assemblage garnet–kyanite–zoisite–staurolite–chlorite–plagioclase in the migmatic gneiss series (see Fig. 4), and at higher pressures >12 in albite gneiss series of the Kardamos Complex. Lithologies of the lower unit with pre-dominant high-grade orthogneisses and migmatites indicate a continental origin.

Intermediate unit

The intermediate unit is composed mainly of amphibolite facies metasediments (Fig. 4). Ultrabasic bodies at different stratigraphic levels represent remnants of an ophiolitic association (Kozhoukharova 1984; Kolcheva and Eskenazy 1988).

On the northwestern flank of the dome, the intermediate unit comprises from bottom to top, (1) thin units of pelitic schists and paragneisses with subordinate amphibolite and marble intercalations at the base. The mineral assemblages of the schist layers are biotite–garnet ± kyanite ± plagioclase ± muscovite; (2) a thick unit of amphibolite interlayered with a few gneiss lenses; (3) thick heterogeneous metacarbonate rocks dominated by pure and impure marble, calc-silicate schist, and thin layers of amphibolite and varied gneisses in the upper part of the section. At some localities, the fine and regular layering of alternating quartzo-feldspathic/pelitic metasediments suggests a turbiditic origin. Strongly sheared metaconglomeratic interbeds may indicate partially preserved basal intervals of turbiditic sequences whose primary lithologic contacts are transposed into the metamorphic layering.

On the southeastern flank, the sequence consists of (1) garnet–kyanite ± staurolite schists with decimetre-scale to metre-scale amphibolitized eclogite lenses; (2) interlayered amphibolites, marbles and gneisses with metagabbros and orthogneisses; (3) strongly dismembered metaperidotites. The structural position of this sequence (Figs. 3, 4) and the presence of eclogite relics in amphibolites and high-grade mineral assemblages in metapelites suggest that this part of the section corresponds to the lowest stratigraphic levels of the intermediate unit. The distinction between lithologies assigned to

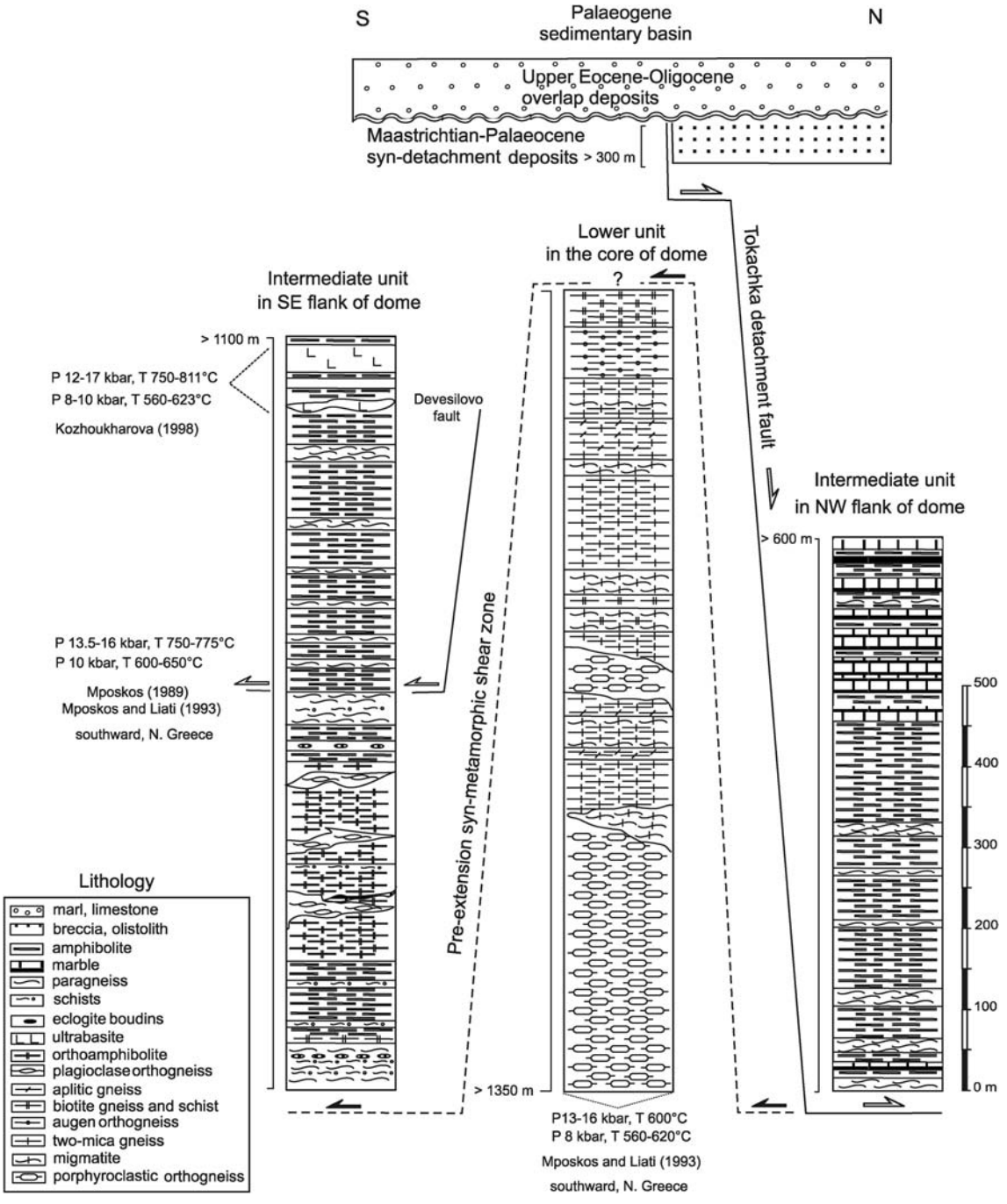

Fig. 4 Generalized stratigraphic columns and structural relationships of the litho-tectonic units. *Large open half-arrow* Tokachka detachment, *small open half-arrow* Devesilovo fault, *solid half-arrow* inferred pre-extension syn-metamorphic shear zone. P–T data explained in text and Fig. 2

the intermediate unit or to the lower unit is based on the lack of marbles and metagabbros in the lower unit. The lithologic differences of the intermediate unit on both flanks of the dome are due to the faults—the Tokachka detachment and Devesilovo fault, respectively, cutting through different parts of the metamorphic sequence and exposing separate stratigraphic levels.

The mixed character of para-protoliths and ortho-protoliths, the occurrence of metaophiolites and trace and rare earth elements geochemistry of metabasic rocks showing immature island arc origin (Haydoutov et al. 2001), collectively, suggest a marginal oceanic basin/arc tectonic environment for pre-cursor lithologies, as also was inferred by the latter authors.

Upper unit

The upper sedimentary unit consists, from bottom to top, of Maastrichtian–Paleocene sediments of the Kru-

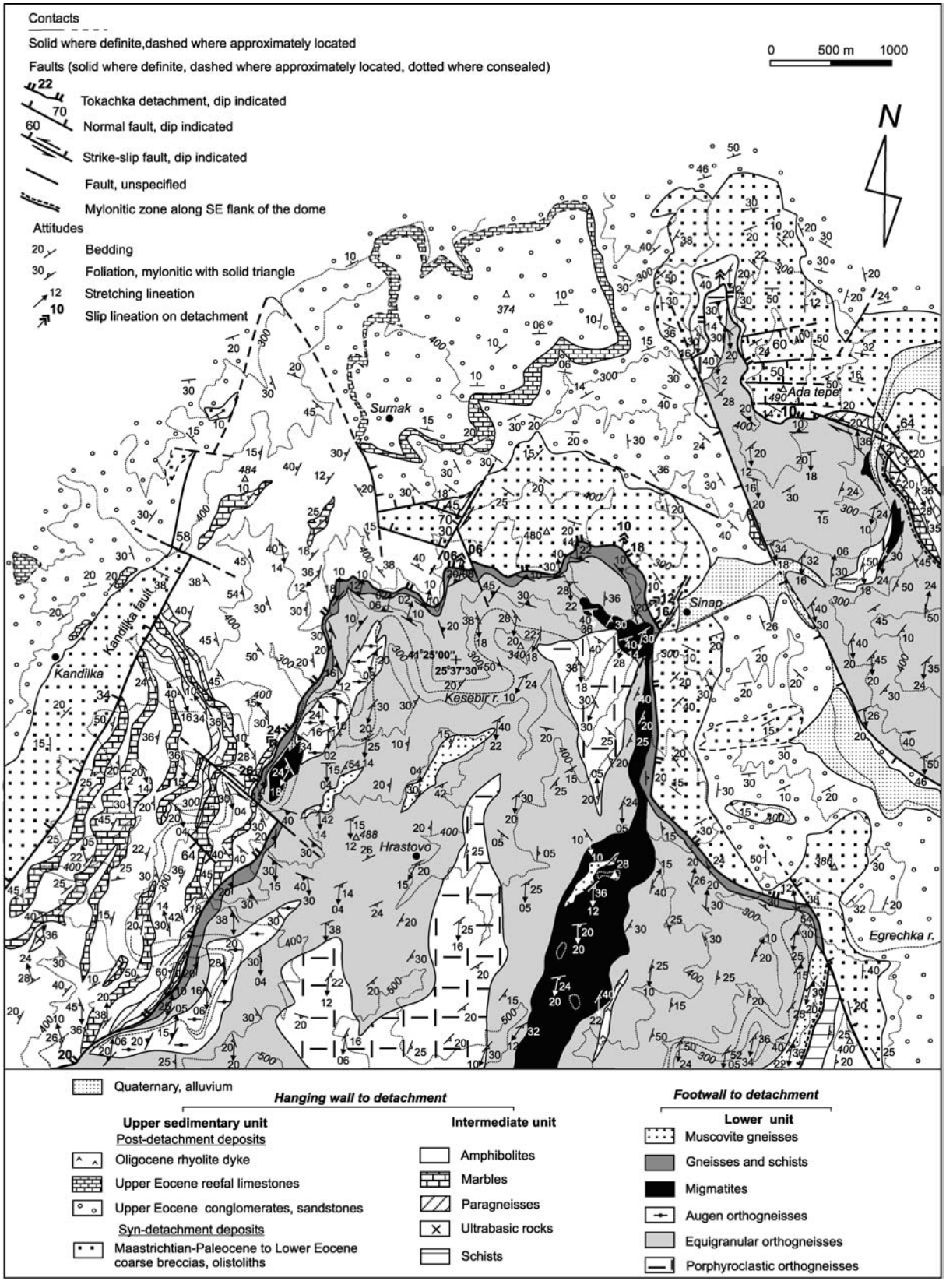

Fig. 5 Geological map of the northern part of the Kesebir–Kardamos dome, showing relationships between detachment, footwall and hanging wall units

movgrad Group (Goranov and Atanasov 1992) and unconformably overlying Upper Eocene–Oligocene sediments, the latter interbedded upsection with volcanic flows and volcano-sedimentary rocks (Boyanov and Goranov 2001 for review). The Krumovgrad Group accumulated in supra-detachment half-grabens filled with several-hundred-meters-thick colluvial–proluvial sediments. They consist of coarse breccias with boulders up to 3–4 m in diameter and large (decametric) slide blocks of the metamorphic basement (only from the intermediate unit), mainly at the base, interstratified upsection with thin conglomerate and sandstone, marl and clayey limestone beds that contain phytofossils of Maastrichtian to Ypresian age. The clastic sediments lie directly with faults making the basal contact, on the Tokachka detachment mylonites or occur adjacent to the detachment surface along its map trace as a supra-detachment basin. These structural and map relationships suggest geometrical compatibility between the detachment and the supra-detachment basin and hanging wall sedimentation accompanied detachment activity. The relationships between hanging wall sediments and the detachment are best portrayed in the northern part of the dome (Fig. 5). There, an up to 800-m-thick Upper Eocene to Oligocene sedimentary succession consist in ascending order of lacustrine red–violet conglomerate (basal Priabonian strata), coal-sandstone and marl-limestone suites that unconformably overlap coarse-clastic lacustrine Maastrichtian–Paleocene deposits in the basin fill and transgressively cover the metamorphic basement in the north (Fig. 3). The late Eocene–Oligocene sediments clearly post-date the detachment surface (Figs. 5, 6). Intermediate to acid volcanic dykes that cut through all lithologies belong to the widespread Oligocene volcanic activity (Marchev et al. 1998, 2003).

Structural observations

Ductile fabrics in the lower unit

The foliation pattern in the lower unit typically wraps around the gneiss core and dips outwards to delineate the dome-shaped culmination (Fig. 7). Exceptions to this attitude include steep foliations in the core due to upright parasitic folds inherent to its hinge zone and drag folding against late faults. Oriented biotite and muscovite, quartz ribbons and, less commonly, flattened feldspar porphyroclasts define the main foliation. In migmatites, the foliation is parallel to the migmatitic layering. This regional (S1) foliation is transposed in isoclinal folds associated with an axial planar crenulation cleavage (S2) in the detachment zone (Fig. 7). The *S* (1 + 2) foliation intensifies upward and becomes mylonitic (Sm). These relationships suggest that S1/Sm are intimately related and control the domal pattern of foliation trajectories.

Strongly oriented mica flakes and elongated quartz–feldspar aggregates define the mineral-stretching lineation, which is consistently oriented NNE–SSW with shallow plunges (Fig. 8). Asymmetric folds in migmatites have strongly attenuated limbs and thickened hinges, and those in the orthogneisses range from close to tight, sub-isoclinal folds. These folds have axes slightly oblique to the stretching lineation in migmatites and consistently parallel to the lineation in orthogneisses (Fig. 8). The rotation from fold hinges oblique to the

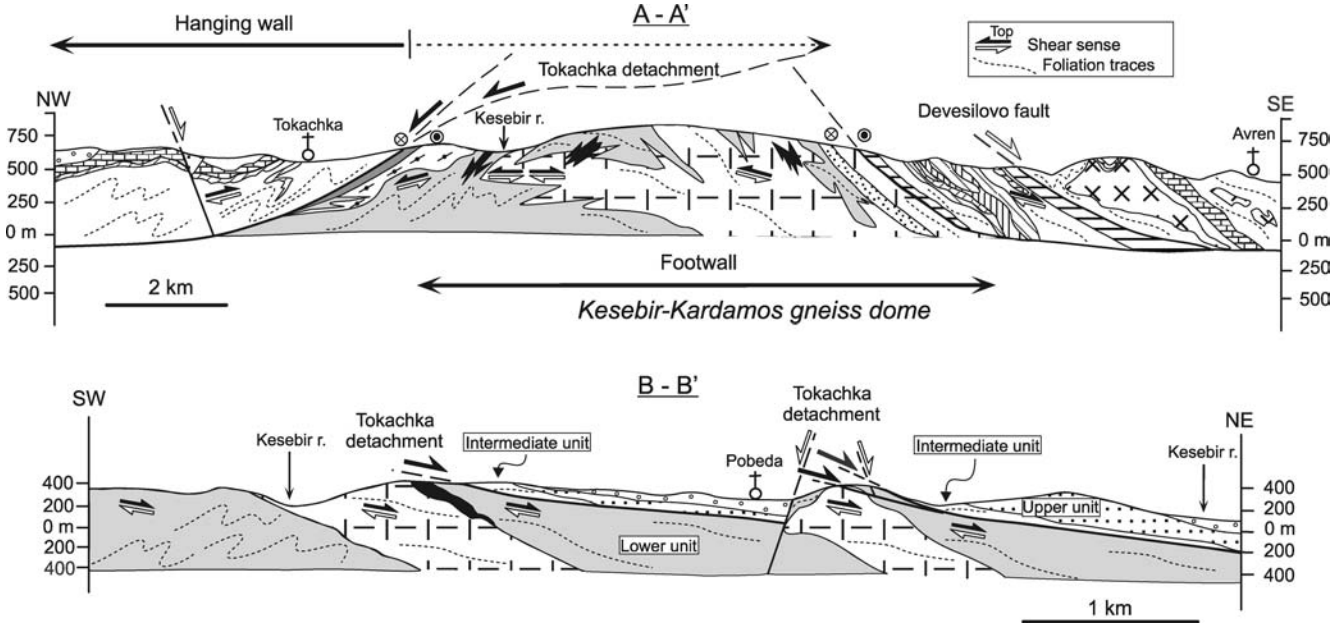

Fig. 6 Cross-sections of the Kesebir–Kardamos dome located in Fig. 3 and showing the dome structure with elements of detachment fault system. Ornaments as in Fig. 3

stretching lineation in the deeper core to dominantly parallel in the detachment mylonite probably reflects upward-increasing shear strain.

Kinematic indicators are abundant and unequivocally demonstrate a consistent top-to-the NNE sense of shear (Fig. 8). Strain localization produced numerous discrete shear zones with top-to-the NE shear on northwest-dipping (Fig. 9a) and top-to-the SW on some south-dipping zones, and sets with both polarities in individual shear zones. Leucosome veins entering shear zones show that partial melting was synchronous with and outlasted the ductile shear zones. Partial melting is consistent with decompression of the lower unit, before cooling below 350°C of the lower unit rocks at ~ 38 Ma (see Table 1).

Fabric elements of the Tokachka detachment and underlying mylonite shear zone

The mylonitic foliation Sm is flat-lying and dips to the north-northwest or north-northeast (Fig. 7). Elongated mineral grains, streaky mica flakes and quartz–feldspar aggregates define the pervasive stretching lineation. Its regionally consistent trend can be traced across the mylonite shear zone underlying the brittle detachment (Fig. 8).

Shear sense indicators systematically indicate top-to-the NNE shear, i.e. north-side-down, parallel to the lineation (Figs. 8, 9b). Asymmetrically tight, occasionally recumbent isoclinal folds have axes that vary from oblique to parallel to the lineation. They are interpreted

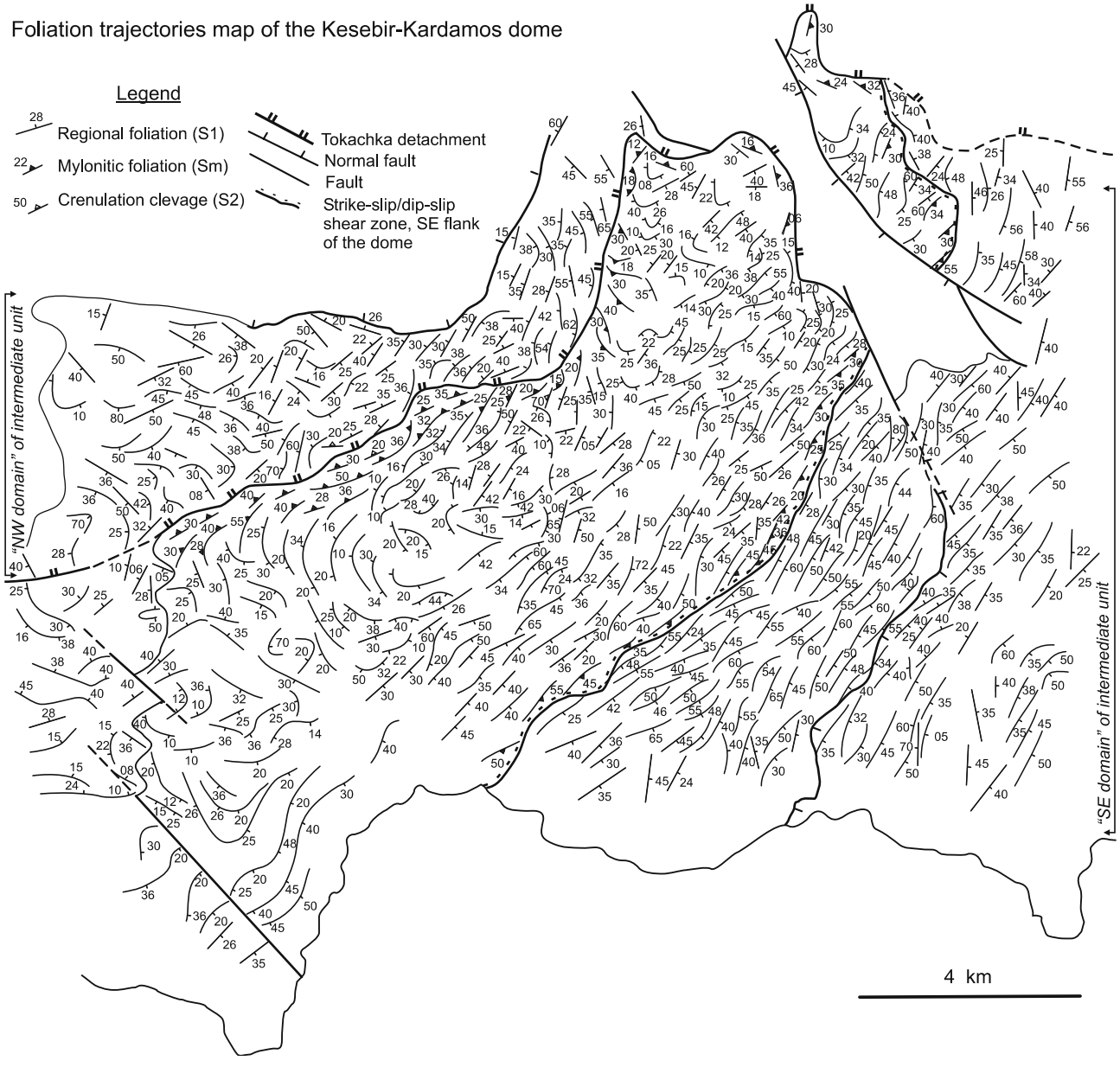

Fig. 7 Map of foliation trajectories in the metamorphic units of the Kesebir–Kardamos dome

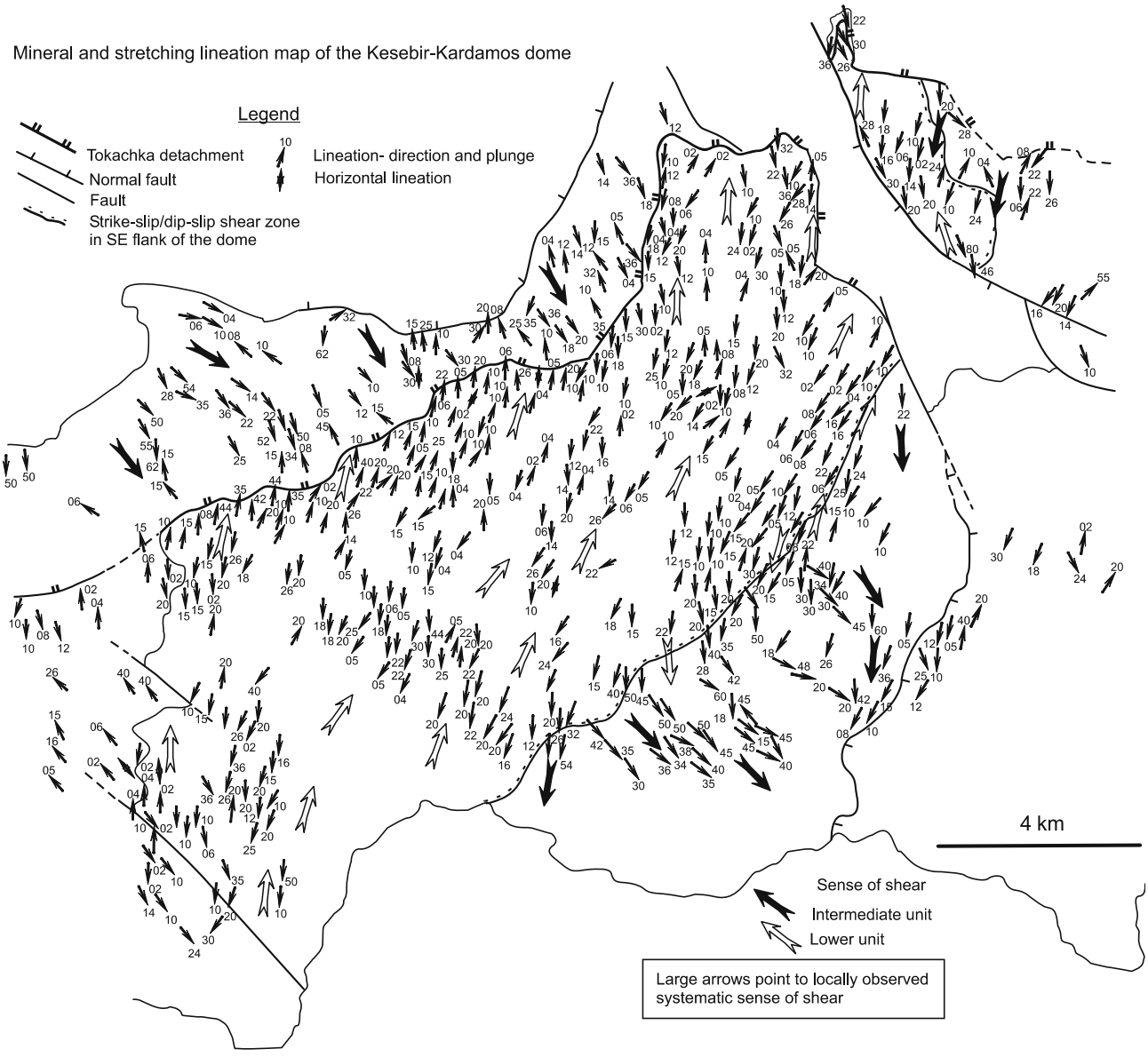

Fig. 8 Mineral and stretching lineations map of the Kesebir–Kardamos dome. *Black arrows* point to the sense of shear on inferred thrust movement within the intermediate unit, *white arrows* in the lower unit are point in the direction of shear associated with extensional deformation

as initially formed north-vergent drag folds, whose axes were rotated toward the kinematic direction during shearing. Folds with lineation-parallel axes are locally decametric. Strain localization produced centimetre-thick ultramylonite bands in S/C mylonitic fabrics and reduced fold limbs.

Deformation/crystallization relationships indicate that NNE-directed shearing took place during the waning stage of amphibolite facies metamorphism and lasted into greenschist facies conditions. Biotite–garnet–kyanite ± staurolite–plagioclase–quartz assemblages in metapelites break down to chlorite–muscovite ± epidote–albite–quartz. Garnet is replaced by secondary white mica and oxides, staurolite and kyanite are altered to sericite and biotite is chloritized close to the detachment surface. In mylonitic gneiss, strain-dependent retrogression produced fine-grained chlorite-white mica aggregates along shear bands within the matrix and sericitization of feldspar porphyroclasts.

The detachment zone exhibits successive overprinting of ductile fabrics by brittle–ductile then brittle structures, compatible with progressively lower temperatures during deformation. The mineral and stretching lineations in mylonites and slickenside striations on brittle surfaces are mostly collinear (Figs. 8, 10a). In addition, brittle senses of shear deduced from fault plane structures, mesoscopic offsets, brittle and semi-brittle shear bands (Fig. 9c), are consistently top-to-the NNE, which suggests kinematic continuity from ductile to brittle conditions during cooling of footwall rocks of the

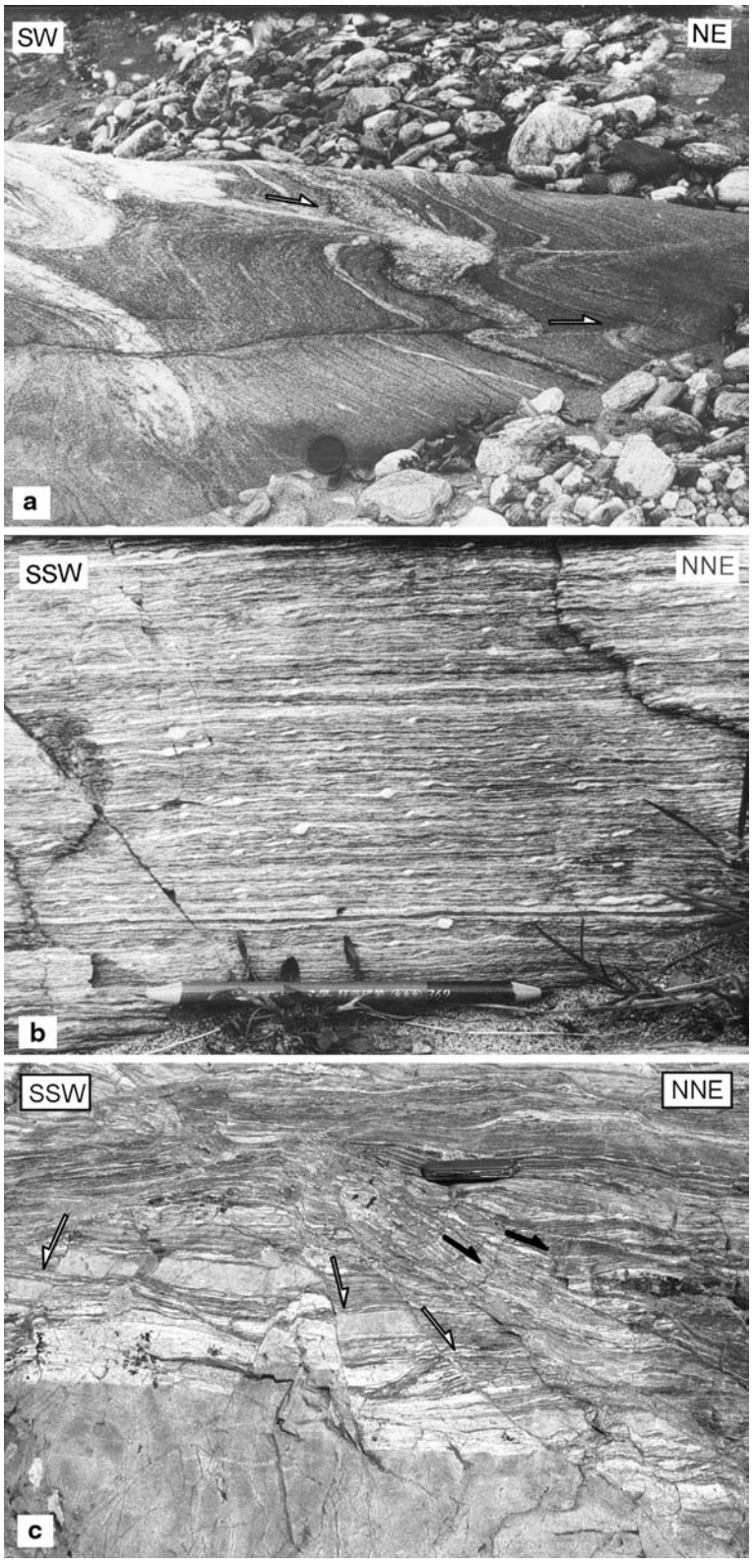

Fig. 9 Ductile fabrics and shear criteria in the lower unit: **a** N-dipping shear zones (*half-arrows*) in migmatites. **b** Exposure parallel to the lineation and orthogonal to the foliation of augen orthogneiss with strong foliation and pronounced stair-stepping K-feldspar porphyroclasts geometry indicating top-to-the NNE shear. **c** Brittle microfaults (*white half-arrows*) superposed on ductile shears (*black half-arrows*) with top-to-the NNE–NE sense of relative movement

detachment fault system. Ductile shearing ceased shortly after 37 Ma, broadly at the same time as brittle deformation began at 35 Ma, which is constrained by $^{40}Ar/^{39}Ar$ ages on hydrothermal adularia crystallized in open spaces provided by high-angle faults in the hanging wall of the detachment (Marchev et al. 2003 2004b; see Fig. 3, Table 1). We therefore attribute ductile and brittle structures to one deformation continuum.

A low-angle normal fault, the Tokachka detachment (Bonev 1996), bounds the north-northwestern side of the

dome (Fig. 3), and can be traced from south of the town of Krumovgrad southwestwards for 15–20 km. It is best exposed along the northern side of the dome (Fig. 5). At Ada Tepe (Fig. 5), the low-angle attitude of this fault is demonstrated by exploration drilling, which constrains the geometry of synthetic high-angle faults that sole at depth into the main detachment surface (e.g. Marchev et al. 2004b, Fig. 4). The gently (8–10°) NE-dipping detachment that can be traced in the field separates gently to moderately (14–36°) SSW-dipping Paleocene hanging wall strata with or without thin slivers of the intermediate unit underneath from mylonitic gneiss in the footwall. West of the village of Sinap, hanging wall strata dip 10–20° southwest towards a 16–18° northeast-dipping fault marked by up to 2-m-thick cataclasites laying on mylonitic footwall rocks (Fig. 11). The fault is best exposed west of Sinap and south of Surnak, where it dips only few degrees (up to 06°) to the north-northeast and has similar expression as at Sinap. There, hanging wall rocks are cut by numerous high-angle normal faults. Farther south and southeast of the village of Kandilka, the detachment cuts down section, separating Paleocene strata and intermediate unit of the hanging wall from a several-meters-thick microbreccia and gouge zone and 20–30° WSW–WNW-dipping mylonitic footwall rocks. At those best-exposed sections, the detachment surface contains down-dip striations (Fig. 10a), small and large-scale corrugations parallel to the striations and brittle offsets indicating NNE-ward movement. Paleocene hanging wall strata show an overall SSW-tilt consistent with syn-depositional rotation of hanging wall strata above the NNE-dipping detachment.

NW–SE and NE–SW-striking faults cross-cut ductile fabrics (Figs. 5, 10b). They display normal and strike-slip senses of movement coeval with or subsequent to the detachment activity. Generally, NE–SW-striking fault set appears to be a broadly contemporaneous expression of brittle deformation at higher structural levels above the detachment, whereas the other fault set crosscuts the detachment surface and NE–SW-trending faults as well, as demonstrated by the map pattern (Fig. 3).

NE-striking high-angle normal faults in the hanging wall show domino-style offsets and block-tilting. Moderately dipping normal faults also occur at the top of the footwall, truncating the mylonitic foliation and reworking previous ductile shear bands. Late kinks and chevron folds with subhorizontal axes trending SSW–NNE appear to be associated with this fault set (see below).

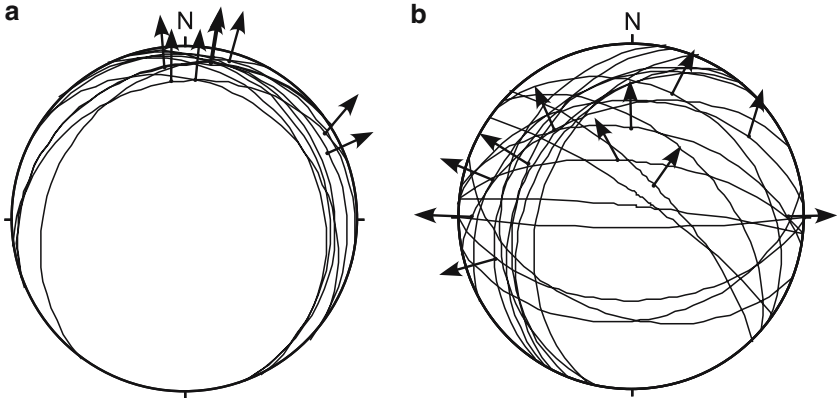

Fig. 10 Lower hemisphere, equal-area stereographic projections of detachment fault planes and slip direction (*arrow* movement of hanging wall) from striations on fault surfaces in **a** and **b** associated upper crustal brittle fault planes and slip data

Fig. 11 **a** Exposure of the Tokachka detachment surface (*foreground*), forming the sharp contact between footwall ductile mylonites of extensional shear zone, cataclasites of intermediate unit and basal breccias of upper unit (*background*) in the hanging wall. *Thick arrow* indicates direction of slip on the detachment as deduced from the slickenside-striations. Width of exposure is more than 30 m

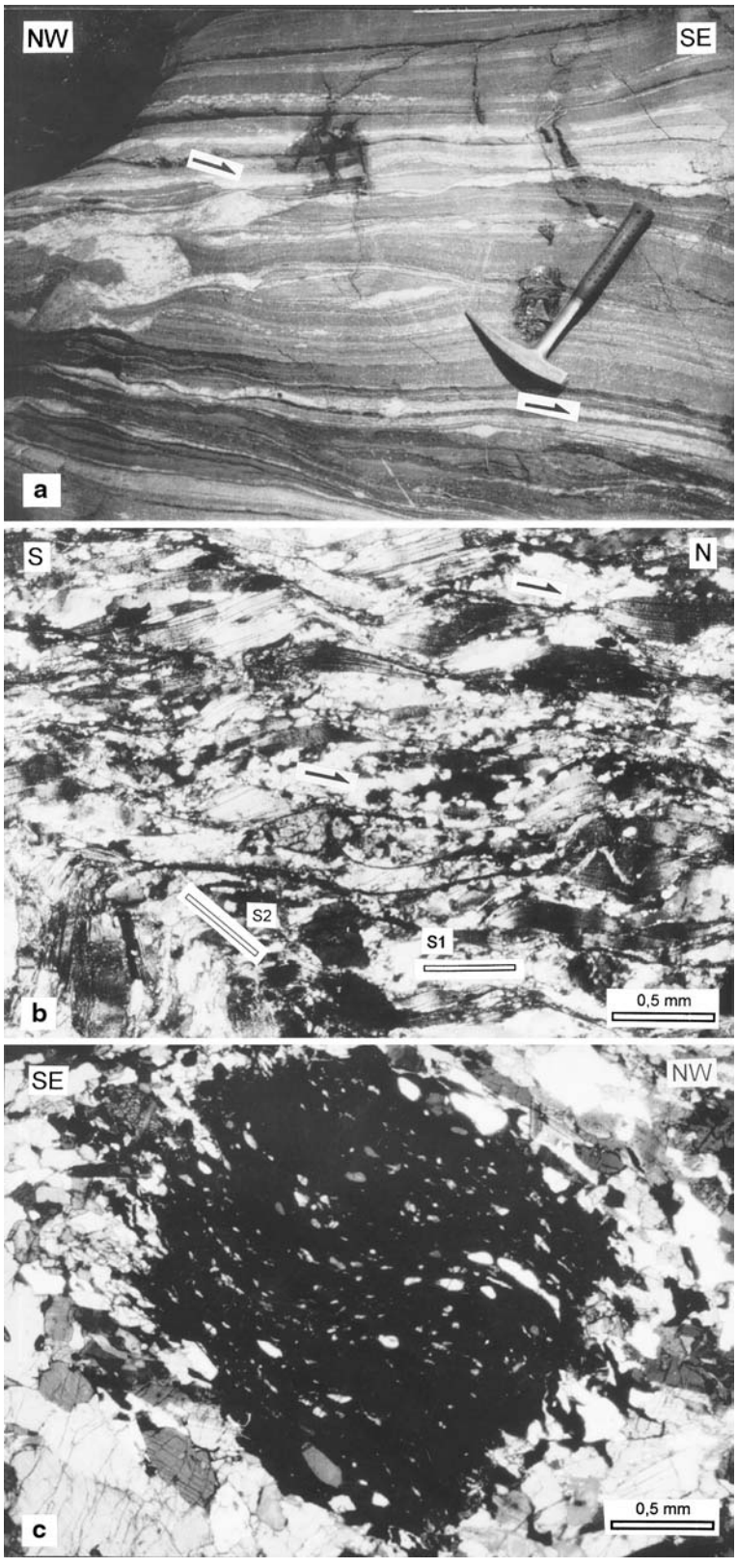

Fig. 12 Ductile deformation and kinematic indicators in the intermediate unit: **a** Asymmetric boudinage, shear bands and sigmoidal aggregates (*arrows*) in intercalated amphibolites, calc-schists and marbles; northwestern domain. **b** Microphotograph of overprinting ductile fabrics. Top-to-the N shear bands and associated "mica fishes", leading to transposition and folding of earlier S1 foliation with development of axial planar S2 crenulation cleavage; northwestern domain. **c** Garnet porphyroblast in section parallel to lineation with helicitic inclusion trails of quartz ± amphibole ± epidote, indicating syn-kinematic growth and anticlockwise rotation, i.e. sense of shear = top-to-SE; southeastern domain

The latest fault set strikes NW and includes mainly high-angle normal faults and late strike-slip faults. They accommodated further brittle extension and typically border small NW–SE oriented graben (south of Ada Tepe hill) with Upper Eocene sedimentary fill (Figs. 3, 6).

Fabric elements of the intermediate unit

Northwestern domain

In the hanging wall intermediate unit on the northwestern flank of the dome the main foliation, which is axial planar to mesoscopic intrafolial folds and occasionally isoclinal rootless folds, generally strikes NE–SW and dips moderately to the NW and SE (Fig. 7). Local variations in foliation attitude are due to later folding. The foliation contains a mineral lineation defined by elongated and stretched grains and mineral aggregates and mineral fringes on garnet porphyroblasts. The lineation is consistently oriented NW–SE and plunges in both directions (Fig. 8). S–SW-vergent, closed to tight folds are generally parallel to the mineral lineation. Late deformation scattered foliation and fold axes define an axis shallowly plunging to the SW (Fig. 7).

Shear sense indicators in outcrops and thin sections oriented parallel to the lineation and perpendicular to the foliation (XZ sections of finite strain), yield a regionally consistent top-to-the SE sense of shear (Fig. 12a), parallel to the lineation (Fig. 8). At the base of the intermediate unit, immediately above the brittle detachment, asymmetric microstructures indicate top-to-the N–NNW sense of shear. In thin sections, a penetrative SE-directed tectonic fabric is cut by N-dipping shear bands with top-to-the N–NNW shear sense (Fig. 12b). These shear bands deform the main foliation, which is consistent with N–NNW-directed brittle–ductile shear taking place during cooling.

Southeastern domain

In the intermediate unit exposed in the southern flank of the dome, the foliation usually strikes NE–SW and dips moderately to the SE or E–SE at the northeastern extremity of the dome (Fig. 7). The foliation contains a mineral and/or stretching lineation defined by elongated and extended mineral grains and aggregates. Mineral lineations pre-dominantly trend NE–SW (Fig. 8) and swing to NW–SE in deepest structural levels. No overprinting relation of lineations with different orientations could be observed. This lineation pattern likely reflects vertically partitioned flow directions in separate structural levels within the intermediate unit, and along rheologically contrasting lower/intermediate unit interface. Scarce mesoscopic folds are upright tight to closed asymmetric folds with hinges subparallel to the dominant lineation trend. Shear sense criteria indicate a consistent top-to-the S–SE sense of shear (Figs. 8, 12c).

NW–SE lineations and small-scale fold axes associated with top-to-the SSE kinematic indicators are reoriented to N–S trends close to the Tokachka detachment, especially in northwestern domain. This reorientation likely reflects passive rotation into the bulk shear direction of mylonites associated with the detachment. Deformation/crystallization relationships such as crystallizations in pressure shadows around garnet porphyroblasts, syn-tectonic staurolite and kyanite porphyroblasts, and micas indicate that ductile structures formed during amphibolite facies of medium-pressure type metamorphism.

Southeastern contact between lower and intermediate units

The contact between the lower and intermediate units is also mylonitic (Fig. 3). This contact differs from the mylonitic Tokachka detachment, by its mylonites showing weaker ductile strain localization, by the lack of ultramylonite bands and penetrative S/C fabrics and the absence of ductile then brittle deformation transition. In addition, kinematic indicators in this contact show both top-to-the NE up-dip and top-to-the SW down-dip shear senses (Fig. 8). However, top-to-the S to SSW-directed criteria are dominant.

Our interpretation is based on several observations: (1) At the base of the intermediate unit, asymmetric microstructures indicate top-to-the SSE non-coaxial flow, contrasting with ubiquitous top-to-the NE ductile shear in footwall orthogneisses, below the Tokachka detachment. (2) Mylonites do not show their original attitude owing to late tilting and upward-bending of the Tokachka detachment footwall. (3) Both metamorphic units display similar amphibolite facies assemblages showing no metamorphic break across the contact. (4) Mostly steep as well as moderately SSE-dipping brittle faults with thin gouge zones locally occur immediately above the mylonitic contact, which suggests a bowed-up and abandoned segment of the Tokachka detachment. The moderately SE-dipping Devesilovo fault in the southeastern domain of the intermediate unit is similar in attitude to the detachment surface in northern Greece (e.g. eastern Kardamos detachment), most likely representing its extension in the Bulgarian part of the dome. The Devesilovo fault cut through the intermediate unit leading to greenschist-facies retrogression of amphibole to actinolite and chlorite in the fault zone without associated ductile strain in the latter both below and above it, and only small-scale fractures and extensional-type kink-bands attest for the brittle deformation in its hanging wall. In the field, immediate continuation or cross-cutting relationships between the Tokachka detachment and Devesilovo fault cannot be observed in southeastern flank of dome, implying no connection with the eastern Kardamos detachment in Greece, respectively. The only connection, acquired later, between both former faults is through a steep normal fault bounding the southwestern side of superimposed obliquely NW–SE trending graben above the Tokachka detachment south of the Sinap (Figs. 3, 5). Nevertheless, the Devesilovo fault possibly merges at depth with the Tokachka detachment judging from the structurally higher position within the detachment footwall assisting its unroofing.

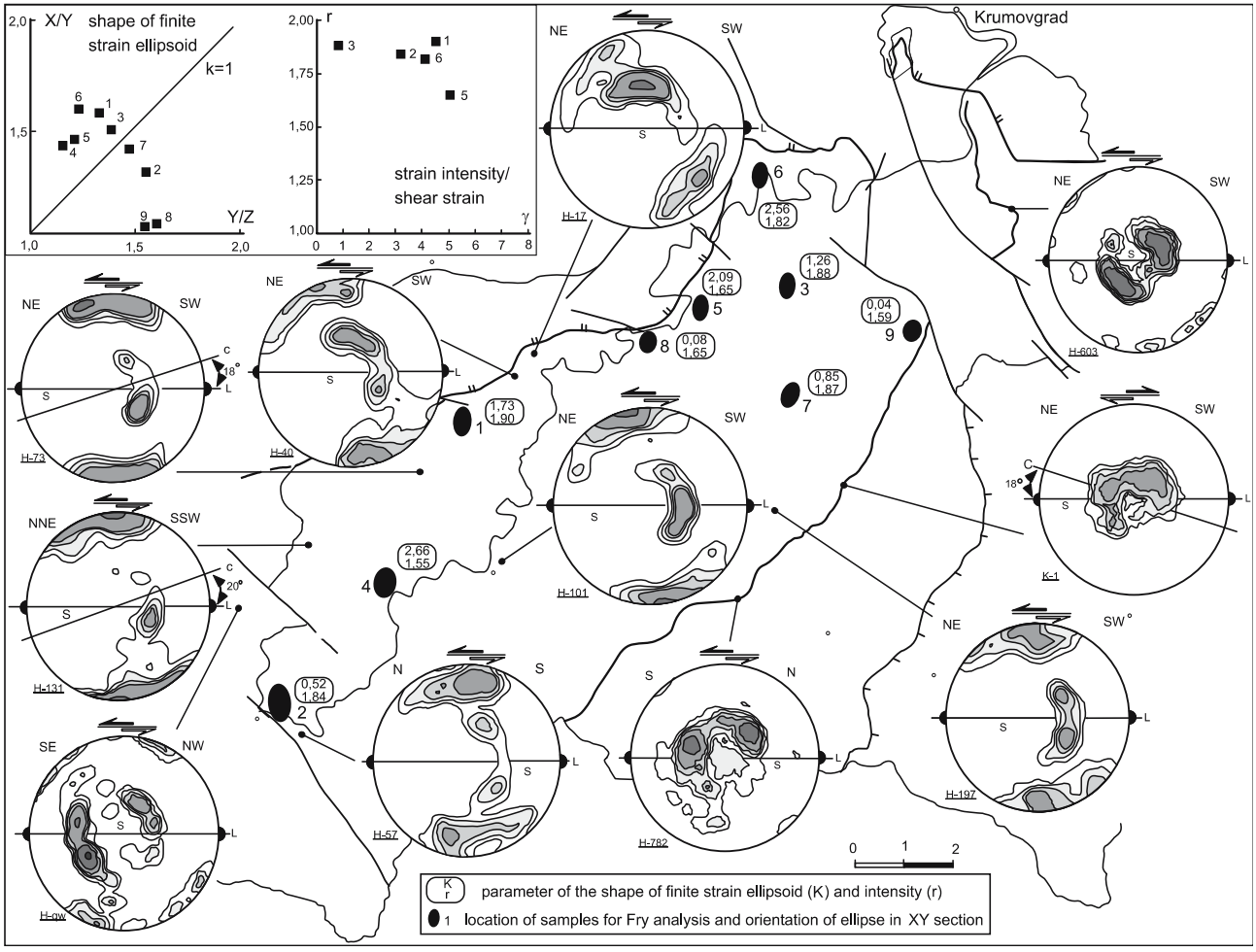

Fig. 13 Finite strain determination and quartz *c*-axis fabrics used to strain analysis. *Inset* related plots of finite strain data. $r=(X/Y)+(Y/Z)$-1 is after Watterson (1968). Numbers of samples for quartz *c*-axis fabrics correspond to that referred in the text. Deduced shear sense is indicated, 240 *c*-axis per diagram, contours: 1–2–3–4–6%.

We interpret the southeastern boundary of the dome as a reactivated, pre-extension ductile shear zone suggesting deeper level syn-metamorphic thrusting between lower and intermediate units, which later evolved as dextral strike-slip zone during final doming as indicated by the foliation–lineation pattern and opposite shear senses below and above the contact (Figs. 7, 8).

Strain analysis

Finite strain determination

The Fry method (Fry 1979) has been applied using K-feldspar porphyroclasts in orthogneisses to provide a measure of strain accumulated during footwall deformation along the detachment fault. The stretching lineation is taken as the *X*-axis on the foliation, *XY* plane orthogonal to the *Z* axis. At least two orthogonal sections in *XZ* and *YZ* planes or *XY* planes of finite strain in outcrops and polished samples were combined to complete the strain determination of the finite strain ellipsoid (X/Y, Y/Z, X/Z).

Measured sites are given in Fig. 13. Most of the finite strain ellipsoids plot in the constrictional field ($K>1$) and near the line $K=1$ (plane strain). The strain intensity $r=(X/Y+Y/Z)$-1 (Watterson 1968) varies between 1.55 and 1.90 and higher values are recorded in the samples that yielded highest shear strain $\gamma>4$–5 ($\gamma=2/\tan 2\theta$, Ramsay and Graham 1970). Two areas can be distinguished. In the detachment zone, prolate ellipsoids are related to most intense strain ($r\sim2$) in samples with equivalent shear strain ($\gamma>5$), deduced from S/C angular relationships, that are compatible with L > S fabrics of tectonites. The central and southwestern parts of the dome are the areas of flattening strain or close to plane strain as evidenced by oblate finite strain ellipsoids.

In summary, constrictional strain in the detachment zone reflects intense deformation whereas flattening and/or near plane strain in the core relate to the component of ductile flow vertical shortening within the crest of the dome.

Kinematic indicators showing opposite senses of shear along the southeastern contact may indicate coaxial deformation. To evaluate this interpretation, we used the approach developed by Wallis et al. (1993). In general shear, particles with an aspect ratio above a critical value rotate until they reach a stable position, whereas those below the critical value rotate randomly (Ghosh and Ramberg 1976; Passchier 1987). Critical aspect ratios are thus related to the degree of non-coaxiality, i.e. vorticity Wm (Passchier 1987). Rotation angles between long axes of K-feldspar porphyroclasts with respect to foliation and aspect ratios Rc of these porphyroclasts were measured on *XZ* profiles of two augen gneiss. The values of Rc are 2.40 and 3.00 (Fig. 14), which are equivalent to vorticities of 0.7 and 0.8, respectively, confirming that the ductile shear regime included a component of coaxial deformation.

Quartz *c*-axis fabrics

To assess kinematics of crystal-plastic flow and its relevance to the lineation in studied tectonites, quartz *c*-axes were measured with a universal stage in *XZ* sections of quartz-rich samples within and at dome-bounding tectonic contacts (Fig. 13). Quartz grains and aggregates show internal strain features (undulose extinction, deformation bands, irregular and serrated grain boundaries) typical of recrystallization under crystal-plastic deformation. Elongated ribbons of recrystallized quartz grains define the microscopic foliation. In some samples, recrystallized quartz grains display a grain-shape fabric oblique to the foliation in a direction consistent with mesoscopic senses of shear. Quartz *c*-axis fabrics are grouped into two basic girdle patterns, according to the similarity of known bulk skeleton.

(1) Single girdle c-axis fabrics

The predominant *c*-axis fabric pattern is characterized by *c*-axes in incomplete (H-40, H-17) to complete (H-57) girdles, and partial cross-girdles (H-qw) with non-uniform *c*-axis populations. The *c*-axis concentration near *Y* is generally low and girdles are seldom connected. The girdle obliquity with respect to the *Z* axis decreases from the core of the dome to the detachment zone, which is consistent with strong strain intensity in mylonites indicated by small angles between shear planes and foliation (H-73, H-131). The obliquity and pronounced asymmetry of girdles with respect to the macroscopic fabric support the shear sense deduced from independent asymmetric kinematic indicators. The pattern of this fabric type involves slip from both basal <a> and prism <a> systems, with contribution of the rhomb <a> system (Schmid and Casey 1986; Wenk 1994).

(2) Single maximum distribution

The single maximum type of *c*-axis pattern (H-782, H-603, K-1) consists of a pronounced maximum centred at or close to Y (Fig. 13), which tends to split into double maxima within the *YZ* plane (H-782). It may evolve into an incomplete girdle (H-603) oblique to the foliation.

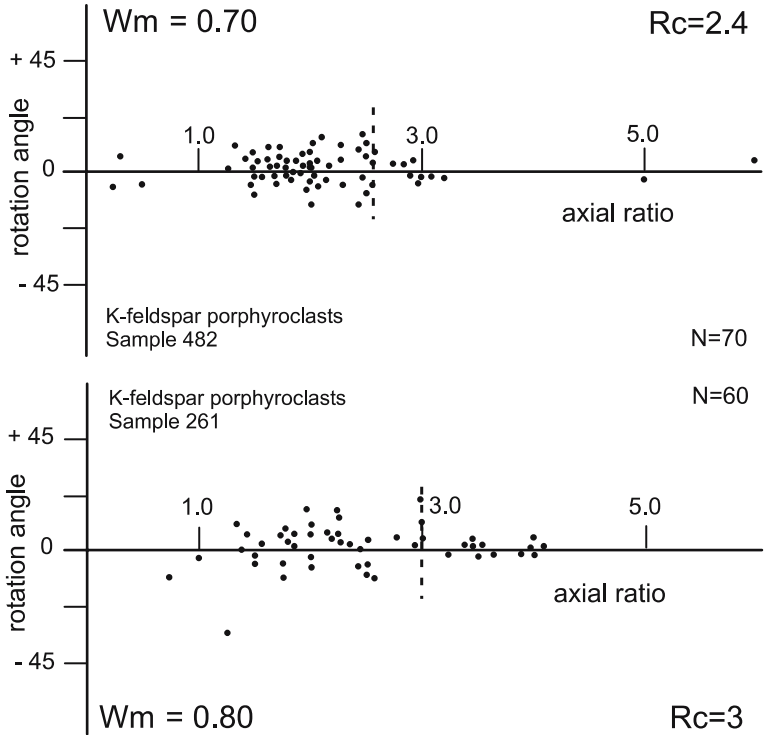

Fig. 14 Plots of aspect ratio against inclination angles of K-feldspar porphyroclasts with respect to main foliation in augen gneiss samples. The *dashed line* defines the critical aspect ratio (*Rc*) of objects with stable position, subparallel to the foliation from non-stable of large scatter in readings. Corresponding value of vorticity Wm = R^2_c-1/R^2_c+1, after Passchier (1987)

The single *c*-axis maximum close to *Y* is attributed to dominant slip on single prism <a> system and, to a minor extent, slip on basal <a> system. This fabric pattern is localized in high-strain zones along the SE contact of the gneiss dome. The asymmetry of fabric skeleton with respect to the foliation, lineation and shear bands consistently agrees with locally observed shear sense in rocks.

In summary, the asymmetry of quartz *c*-axis fabrics shows that fabric acquisition in the Kesebir–Kardamos gneiss mylonites includes a kinematically compatible and significant non-coaxial component of ductile shear. Therefore, the pattern and intensity of quartz *c*-axis fabrics are controlled by the bulk finite strain, and the lineation can be taken as the kinematic direction of crystal-plastic flow.

Tectonic interpretation and discussion

Early crustal contraction

Structural and kinematic data of the earliest, regionally coherent event (i.e. excluding within-clasts information) indicate top-to-the-SSE shear for the earlier deformation event in the intermediate unit, which is absent in the lower migmatite-gneiss unit. Deformation/crystallization microstructural relationships of shear fabrics relative to amphibolite-facies mineral phases in rocks indicate the syn-metamorphic character of this event. We have not been able to relate the mesoscopic fabrics to a particular contraction-linked tectonic contact, although the shear zone at the rear of dome along southeastern contact of the dome core presents many characteristics for syn-metamorphic thrust. This deficiency is due to the effects of subsequent deformation, which controlled the structural pattern of the dome. We assign the pre-dome fabric to pre-latest Late Cretaceous, southeast-vergent thrusting involving oceanic crust (meta-harzburgites and meta-basic rocks), as in the Eastern and Central Rhodope (Burg et al. 1990, 1996; Koukovelas and Doutsos 1990).

Syn-thickening to post-thickening crustal extension

Our structural analysis suggests that the Kesebir–Kardamos dome is related to top-to-NNE–NE extension. This event substantially thinned the intermediate unit, unroofed the lower unit and contributed to the exhumation of the upper and middle part of the Rhodope metamorphic pile, which suggests general extension.

The timing of extensional tectonics in the eastern Rhodope may be considered in the light of stratigraphic information contained in the supra-detachment sedimentary basins and radiometric data on metamorphic minerals. The oldest unmetamorphosed sediments to be affected by low-angle normal faulting are Maastrichtian–Paleocene Krumovgrad Group deposits (Goranov and Atanasov 1992). The chaotic aspect of these deposits, the tectonic origin of marble and amphibolite clasts, blocks and boulders (deformed at borders without or little matrix of the same composition) in direct contact with the detachment, and Maastrichtian and mostly Palaeocene (Monthian–Thanetian) to Lower Eocene (Ypresian) marls and clayey limestones interstratified in the midst of succession with coarse boulder-breccias and olistoliths, are evidence for the onset of extension at the Palaeocene–Eocene boundary. In addition, Paleocene–Lower Eocene deposits, truncated by high-angle normal faults in the detachment hanging wall, are overlain unconformably by flat-lying unfaulted Priabonian breccia–conglomerate suite (Goranov and Atanasov 1992; Boyanov and Goranov 1994). These stratigraphic constraints imply a Lower Eocene upper age limit for extension. In adjoining northern Greece, however, Middle Eocene (Lutetian) limestones and underlying basal conglomerates unconformably rest on metamorphic units and, together with Priabonian–Oligocene volcano-sedimentary sequences, fill small fault-bounded sedimentary basins (Papadopoulos 1982; Karfakis and Doutsos 1995). This suggests that extension initiated earlier on the northern flank of the dome, and later on the southern flank. The Late Cretaceous–Paleocene to Lower Eocene stratigraphic interval in sedimentary sequences broadly corresponds and is slightly younger than the span of ages of medium-pressure to low-pressure metamorphism in the underlying metamorphic rocks (Table 1).

Tectonic model for the evolution of Kesebir–Kardamos dome and geodynamic implications

We propose that the Kesebir–Kardamos dome was exhumed beneath a low-dipping ductile shear zone coupled with brittle faulting at shallow crustal levels. We describe the model as follows (Fig. 15):

Between ca. 119 and 65 Ma (regional geochronology, e.g. Mposkos and Wawrzenitz 1995; Wawrzenitz and Mposkos 1997; Liati et al. 2002; Ovtcharova et al. 2003; Marchev et al. 2004a; see Table 1) SSE-directed shearing accompanying high-pressure/high-temperature and medium-pressure amphibolite facies metamorphism developed during northward subduction of the Vardar Ocean (Fig. 15, upper panel). The time span include Alpine convergence and crustal thickening together with peak metamorphism in the nappe stack radiometrically dated in eclogites and metaophiolites of eastern Rhodope (Wawrzenitz and Mposkos 1997; Liati et al. 2002), intrusion of latest Cretaceous-Palaeocene/Eocene late-tectonic to post-tectonic granitoids (Ovtcharova et al. 2003; Marchev et al. 2004a). The above isotopic data unequivocally indicate that the main contractional tectono-metamorphic event in the eastern Rhodope occurred at least pre-latest Late Cretaceous time, also consistent with sedimentary constraints provided by supra-detachment basin deposits (see below). The record

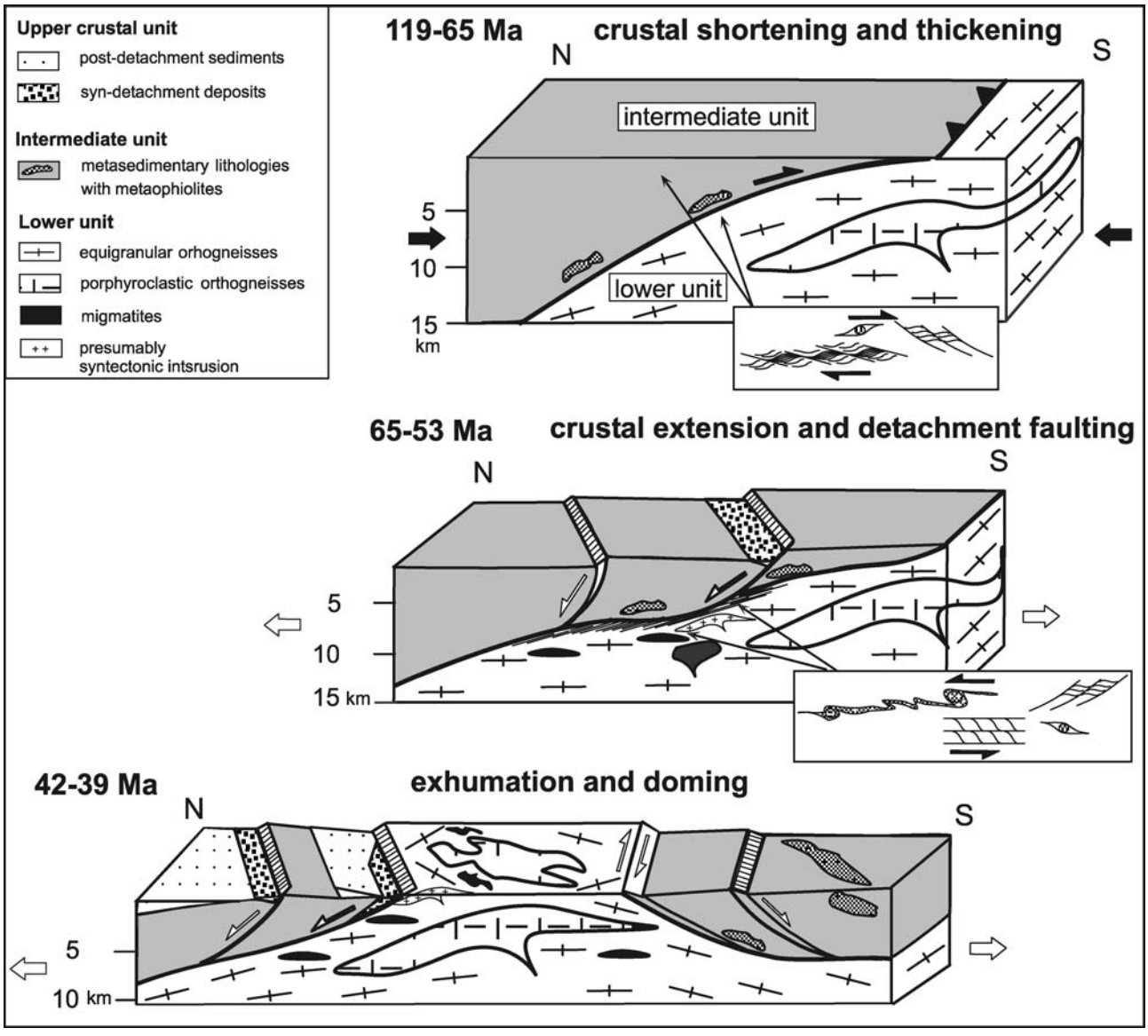

Fig. 15 Tectonic evolutionary model proposed to account for the exhumation of Kesebir–Kardamos dome and its emplacement beneath detachment fault system

of this crustal stacking event can be followed southwestwards into the Serbo-Macedonian and Pelagonian zones (Burg et al. 1995; Lips et al. 1998; Kilias et al. 1999). Thermal relaxation after crustal thickening caused partial melting of mid-to lower parts of the nappe pile, which accompanied their exhumation in the intervening crustal-extension stage.

Extension (ca. 65–35 Ma geochronologic constraints from Lips et al. 2000; Krohe and Mposkos 2002; Marchev et al. 2003; Marchev et al. 2004b), bracketed between syn-tectonic hanging wall sedimentation, mica cooling ages in the detachment footwall and adularia crystallization within faults in its hanging wall (Table 1), initiated with a north-vergent low-angle extensional shear zone at depth coupled with a detachment fault in the upper crustal level (Fig. 15, middle panel) that assisted unroofing of deep structural levels. Palaeocene sediments deposited in half-grabens on the detachment hanging wall include fault-slope breccias and large olistoliths from the intermediate unit. These coarse clastics are interbedded with fossiliferous Ypressian marls and limestones showing that the extension was ongoing in early Eocene times. Subsequent extension led to thinning and unroofing of the intermediate unit, which was exposed by Early Eocene–Middle Eocene times. A normal fault bounding the sedimentary basin to the northwest of the dome, to the east of Kandilka (Fig. 5), may represent a detachment splay that excised the intermediate unit at 46 Ma and later. Up-doming and exhumation of the footwall occurred later as extension

proceeded ca. 42–39 Ma (Fig. 15, lower panel). SE-dipping normal faults cutting through the intermediate unit on the southern side of the dome (e.g. Devesilovo fault correlated with the eastern Kardamos detachment in Greece) accommodate upward bending of the footwall, and contributed to doming and exhumation of the core. Late brittle faulting that accompanied upper crustal extension is constrained at 35 Ma by the adularia age mentioned before (Table 1). Post-detachment sediments are shallow-marine and persisted into Oligocene time, accompanying widespread volcanic activity in the region.

According to this evolutionary model, contractional deformations related to syn-metamorphic crustal stacking in the Rhodope massif were partly contemporaneous with early extension, which in the study area is exemplified by Late Cretaceous–Palaeocene/Eocene granite intrusions and syn-tectonic sediment deposition at shallow-superficial crustal levels. This syn-orogenic character of extensional tectonics is also supported by the climax of collision and Palaeocene closure of the Vardar zone (Ricou et al. 1998). The Kesebir–Kardamos dome formed concurrently with late thrusting stages. We thus link syn-orogenic extension in the upper part of the "orogenic wedge" with continued underthrusting in the foreland, to the south. Extensional tectonics described herein may be related to gravitational adjustment of an unstable wedge (Platt 1986), or to another syn-orogenic instability (Ricou et al. 1998). This syn-collisional extension predates the onset of post-orogenic Aegean extension by ca. 30 m. y. (e.g. Dinter and Royden 1993; Sokoutis et al. 1993; Dinter 1998; Gautier et al. 1999), which further contributed to Miocene exhumation and unroofing of the roots of the Alpine orogenic stack, i.e. the floor of the Rhodope thrust complex.

Conclusions

1. The distinction in origin lithologies and structures of high-grade rocks in the Kesebir–Kardamos dome area allow distinguishing the different structural units.
2. Early deformation is characterized by top-to-the-SSE shear related to syn-metamorphic thrusting, pervasively recorded within the intermediate unit.
3. The dome structure formed during extensional unroofing of the footwall of the detachment fault system. Extension caused attenuation and ductile thinning of the metamorphic pile. In general, the extensional tectonic transport was top-to-the-NNE. Concomitant brittle normal faulting accommodated upper crustal extension during continued ductile flow at deep structural levels.
4. Strain analysis and quartz *c*-axis fabrics of mylonitic gneisses indicate that they suffered a dominant non-coaxial shear regime. Constrictional strain dominates the finite strain pattern and spatially deviates toward plane strain conditions.
5. Crustal extension described in the Kesebir–Kardamos dome started in the Early Tertiary, largely synchronous with closure of the Vardar Ocean and collision in the Rhodope. This syn-collisional extension might be a precursor and/or make a transition to more recent Early Miocene Aegean back-arc extension.

Acknowledgments Constructive reviews from B.C. Burchfiel and D.A. Dinter, their valuable suggestions and critical comments on the manuscript are greatly acknowledged. Part of this work was carried out while NB was holding a scholarship from the French Ministère des Relations Extérieures, in Montpellier.

References

Bonev N (1996) Tokachka shear zone southwest of Krumovgrad in the eastern Rhodopes, Bulgaria: an extensional detachment. Ann Univ Sofia Fac Geol Geogr Liv 1 Geol 89:96–107

Bonev N (1999) Extensional exhumation of metamorphic complexes in the Kesebir dome, eastern Rhodope. EOS Trans AGU 86:1046

Bonev N (2002) Structure and evolution of the Kesebir gneiss dome, eastern Rhodope. Ph.D thesis, University of Sofia, 282pp

Boyanov I, Goranov A (1994) Paleocene–Eocene sediments from the northern periphery of the Borovitsa depression and their correlation with similar sediments in the east Rhodopean Paleogene depression (in Bulgarian, abstract in English). Rev Bulg Geol Soc 55:83–102

Boyanov I, Goranov A (2001) Late Alpine (Palaeogene) superimposed depressions in parts of Southeast Bulgaria. Geol Balc 31:3–36

Brun J-P (1983) L'origine des dômes gneissiques: modèles et tests. Bull Soc géol France 7:219–228

Burg J-P, Ivanov Z, Ricou L-E, Dimor D, Klain L (1990) Implications of shear-sense criteria for the tectonic evolution of the central Rhodope Massif, southern Bulgaria. Geology 18:451–454

Burg J-P, Van Den Driessche J, Brun J-P (1994) Syn-to post-thickening extension: modes and consequences. C R Acad Sci Paris 319(II):1019–1032

Burg J-P, Godfriaux I, Ricou L-E (1995) Extension of the Mesozoic Rhodope thrust units in the Vertiskos-Kerdilion Massifs (northern Greece). Compt Rend Acad Sci Paris 320(IIa):889–896

Burg J-P, Ricou L-E, Ivanov Z, Godfriaux I, Dimov D, Klain L (1996) Syn-metamorphic nappe complex in the Rhodope Massif. Structure and kinematics. Terra Nova 8:6–15

Coney PJ, Harms TA (1984) Cordilleran metamorphic core complexes: cenozoic extensional relics of Mesozoic compression. Geology 12:550–554

Davis GA, Anderson JL, Frost EG, Schakleford TJ (1980) Regional miocene detachment faulting and early tertiary mylonitization, Whipple-Buckskin-Rawhide Mountains. Mem Geol Soc Am 153:79–130

Del Moro A, Innocenti F, Kyriakopoulos K, Manetti P, Papadopoulos P (1988) Tertiary granitoids from thrace (northern Greece): Sr isotopic and petrochemical data. N Jb Mineral Abh 159:113–135

Dercourt J, Ricou L-E (1987) Discussion sur la place de la Bulgarie au sein de système alpin. Rev Bulg Geol Soc 48(3):1–14

Dercourt J, Zonenshain LP, Ricou L-E, Kazmin VG, Le Pichon X, Knipper AL, Grandjacquet C, Sbortshhikov IM, Geyssant J, Lepvrier C, Perchersky DH, Boulin J, Sibuet J-C, Savostin LA, Sorokhtin O, Wesphal M, Bazhrnov ML, Lauer J-P, Biju-Duval (1986) Geological evolution of the tethys belt from the Atlantic to the Pamirs since the Lias. Tectonophysics 123:241–315

Dewey J (1988) Extensional collapse of orogens. Tectonics 7(6):1123–1139
Dewey JF, Sengör AMC (1979) Aegean and surrounding regions: complex multiplate and continuum tectonics in a convergent zone. Geol Soc Am Bull 90:84–92
Dinter DA (1998) Late cenozoic extension of the Alpine collisional orogen, northeastern Greece: origin of the north Aegean basin. Geol Soc Am Bull 110(9):1208–1230
Dinter DA, Royden L (1993) Late cenozoic extension in northeastern Greece: strymon valley detachment system and Rhodope metamorphic core complex. Geology 21(1):45–48
Dinter DA, Macfarlane AM, Hames W, Isachsen C, Bowring S, Royden L (1995) U-Pb and $^{40}Ar/^{39}Ar$ geochronology of the symvolon granodiorite: implications for the thermal and structural evolution of the Rhodope metamorphic core complex, northeastern Greece. Tectonics 14:886–908
Fry N (1979) Random point distributions and strain measurements in rocks. Tectonophysics 60:89–105
Gautier P, Brun J-P, Moriceau R, Sokoutis D, Martinod J, Jolivet L (1999) Timing, kinematics and cause of Aegean extension: a scenario based on a comparison with simple analogue experiments. Tectonophysics 315:31–72
Ghosh SK, Ramberg H (1976) Reorientation of inclusions by combination of pure shear and simple shear. Tectonophysics 34:1–70
Goranov A, Atanasov G (1992) Lithostratigraphy and formation conditions of Maastrichtian-Paleocene deposits in Krumovgrad district. Geol Balcanica 22(3):71–82
Harkovska A, Yanev Y, Marchev P (1989) General features of the Paleogene orogenic magmatism in Bulgaria. Geol Balcanica 19(1):37–72
Haydoutov I, Kolcheva K, Daieva L, Savov I (2001) Island-arc origin of the neoproterozoic variegated formations from the east Rhodopes (Avren synform and Bela Reka antiform), Bulgaria. ESF Europrobe meeting, Ankara, Abs.1:31–32
Hetzel R, Passchier C, Ring U, Dora O (1995) Bivergent extension in orogenic belts: the menderes massif (southwestern Turkey). Geology 23(5):455–458
Hodges KV Walker JD, Wernicke BP (1987) Footwall structural evolution on the Tucki detachment system, Death valley region, southeastern California. In: Coward MP, Dewey JF, Hancock PL (eds) Continental extensional tectonics. Geol Soc Lond Sp Publ 28:393–408
Ivanov Z (1988) Aperçu général sur l'évolution géologique et structurale du massif des Rhodopes dans le cadre des Balkanides. Bull Soc Géol France 8(IV, 2):227–240
Jaranov D (1960) Tectonics of Bulgaria. Technica, Sofia, 283p (in Bulgarian, French abstract)
Karfakis I, Doutsos T (1995) Late orogenic evolution of the circum-Rhodope belt, Greece. N Jb Geol Paläont Mh H.5:305–319
Kilias A, Falalakis G, Mountrakis D (1999) Cretaceous-Tertiary structures and kinematics of the serbomacedonian metamorphic rocks and their relation to the exhumation of the hellenic hinterland (Macedonia, Greece). Int J Earth Sci 88:513–531
Kolcheva K, Eskenazy G (1988) Geochemistry of metaeclogites from the central and eastern Rhodope Mts. Geol Balcanica 18:61–78
Koukouvelas I, Doutsos T (1990) Tectonic stages along a traverse cross cutting the Rhodopian zone (Greece). Geol Rund 79:753–776
Kozhoukharov D (1987) The Rhodopian supergroup in the avren syncline, eastern Rhodopes (in Bulgarian, abstract in English). Geol Balcanica 17:21–40
Kozhoukharova E (1984) Origin and structural position of the serpentinized ultrabasic rocks of the pre-Cambrian ophiolitic association in the Rhodope Massif. I Geologic position and composition of ophiolite association (in Russian, abstract in English). Geol Balcanica 14:9–36
Kozhoukharova E (1998) Eclogitization of serpentinites into narrow shear zones from the avren syncline, eastern Rhodopes (in Bulgarian, abstract in English). Geochem Miner Petrol 35:29–46
Krohe A, Mposkos E (2002) Multiple generations of extensional detachments in the Rhodope Mountains (northern Greece): evidence of episodic exhumation of high-pressure rocks. In: Blundell DJ, Neubauer F, von Quadt A (eds) The timing and location of major ore deposits in an evolving orogen. Geol Soc Lond Sp Publ 204:151–178
Liati A (1986) Regional metamorphism and overprinting contact metamorphism of the Rhodope zone, near Xanthi (N. Greece): Petrology, geochemistry and geochronology, PhD thesis, Tech University of Braunschweig, 186pp
Liati A (1988) Amphibolized eclogites in the Rhodope crystalline complex, near Xanthi (N. Greece). N Jb Miner Mh H1:1–8
Liati A, Mposkos E (1990) Evolution of eclogites in the Rhodope zone of northern Greece. Lithos 25:89–99
Liati A, Gebauer D (1999) Constraining the prograde and retrograde P-T-t path of eocene HP-rocks by SHRIMP dating of different zircon domains: inferred rates of heating, burial, cooling and exhumation for central Rhodope, (N Greece). Contrib Miner Petrol 135:340–354
Liati A, Gebauer D, Wysoczanski R (2002) U-Pb SHRIMP-dating of zircon domains from UHP garnet-rich mafic rocks and late pegmatoids in the Rhodope zone (N Greece); evidence for early cretaceous crystallization and late cretaceous metamorphism. Chem Geol184:281–299
Lips ALW, White SH, Wijbrans JR (1998) $^{40}Ar/^{39}Ar$ laserprobe dating of discrete deformational events: a continuous record of early Alpine tectonics in the Pelagonian Zone, NW Aegean area, Greece. Tectonophysics 298:133–153
Lips ALW, White SH, Wijbrans JR (2000) Middle-late Alpine thermotectonic evolution of the southern Rhodope Massif, Greece. Geodin Acta 13:281–292
Lister G, Banga G, Feenstra A (1984) Metamorphic core complexes of cordilleran type in the cyclades, Aegean sea, Greece. Geology 12:221–225
Macheva LA (1998) 3T-phengites in the rocks of biala reka metamorphic group: an indicator for high-pressure metamorphism (in Bulgarian, abstract in English). Geochem Miner Petrol 35:17–28
Marchev P, Vaselli O, Downes H, Pinarelli L, Ingram G, Rogers G R. Raicheva R, (1998) Petrology and geochemistry of alkaline basalts and lamprophyres: implications for the chemical composition of the upper mantle beneath the eastern Rhodopes (Bulgaria). In: Christofides G, Marchev P, Serri G (eds) Tertiary magmatism of the Rhodopian region. Acta Vulcanol 10:233–242
Marchev P, Singer B, Andrew C, Hasson S, Moritz R, Bonev N (2003) Characteristics and preliminary 40Ar/39Ar and 87Sr/86Sr data of the upper eocene sedimentary-hosted low-sulfidation gold deposits Ada Tepe and Rosino, SE Bulgaria: possible relation with core complex formation, In: Eliopoulos DG et al (eds) Mineral exploration and sustainable development, vol. 2. Millpress, Rotterdam, pp1193–1196
Marchev P, Raicheva R, Downes H, Vaselli O, Chiaradia M, Moritz R (2004a) Compositional diversity of eocene-oligocene basaltic magmatism in the eastern Rhodopes, SE Bulgaria: implications for genesis and tectonic setting. Tectonophysics 393:301–328
Marchev P, Singer B, Jelev D, Hasson S, Moritz R, Bonev N (2004b) The Ada Tepe deposit: a sediment-hosted, detachment fault-controlled, low-sulfidation gold deposit in the eastern Rhodopes, SE Bulgaria. Schweiz Miner Petrogr Mitt 84(1/2):59–78
Meyer W (1968) Alterstellung des plutonismus im sdteil der rila-Rhodope-Masse. Geol Paläont 2:177–192
Meyer W (1969) Die faltenachsen im Rhodopen-Kristallin östlich des strimon (nordost-Griecheenland). Geotekt Forsch 31:86–96
Mposkos E (1989) High-pressure metamorphism in gneisses and pelitic schists in the east Rhodope zone (N. Greece). Miner Petrol 41:25–39
Mposkos E (1998) Cretaceous and tertiary tectonometamorphic events in Rhodope zone (Greece). Petrological and geochronological evidences. Bull Geol Soc Greece 32(3):59–67

Mposkos E, Liati A (1993) Metamorphic evolution of metapelites in the high-pressure terrane of the Rhodope zone, northern Greece. Can Miner 31:401–424

Mposkos E, Wawrzenitz N (1995) Metapegmatites and pegmatites bracketing the time of HP-metamorphism in polymetamorphic rocks of the E. Rhodope, northern Greece: Petrological and geochronological constraints. Geol Soc Greece Sp Publ 4/2:602–608

Mposkos E, Krohe A (2000) Petrological and structural evolution of continental high-pressure (HP) metamorphic rocks in the Alpine Rhodope domain. In: Panaydes I, Xenophontos C, Malpas J (eds) Proceedings of the 3rd international conference geology East Mediterranean, Geol Surv Nicosia, Cyprus 1:221–232

Mposkos ED, Kostopoulos DK (2001) Diamond, former coesite and supersilicic garnet in metasedimentary rocks from the Greek Rhodope: a new ultrahigh-pressure metamorphic province established. Earth Planet Sci Lett 192:497–506

Ovtcharova M, Quadt AV, Heinrich CA, Frank M, Kaiser-Rohmeier M, Peycheva I, Cherneva Z (2003) Triggering of hydrothermal ore mineralization in the central Rhodopean core complex (Bulgaria)-insight from isotope and geochronological studies on tertiary magmatism and migmatisation, In: Eliopoulos DG et al (eds) Mineral exploration and sustainable development, vol. 1. Millpress, Rotterdam, pp367–370

Papadopoulos C (1982) Geological map of Greece, map sheets 1:50 000 (Fere-Peplos-Enos-Maronia-Sappe-Kardamos-Virsini-Derio-Sufli-Didimoticho). IGME Publisher Department, Athens

Passchier C (1987) Stable position of rigid objects in non-coaxial flow—a study in vorticity analysis. J Struct Geol 9:679–690

Peycheva I, Quadt AV (1995) U-Pb zircon dating of metagranites from Byala Reka region in the east Rhodopes, Bulgaria. Geol Soc Greece Sp Publ 4/2:637–642

Peytcheva I, Ovtcharova M, Sarov S, Kostitsin J (1998) Age and metamorphic evolution of metagranitoids from Kesebir reka region, eastern Rhodopes–Rb-Sr isotope data. XVI CBGA Congr Vienna Abstract, p471

Peytcheva I, Kostitsin Y, Salnikova E, von Quadt A, Kamenov B, Klain L (1999) Alpine evolution of the magmatism in the west-Rhodopes: Rb-Sr and U-Pb isotope data. J Conf Abs 4:470

Platt J (1986) Dynamics of orogenic wedges and the uplift of high-pressure metamorphic rocks. Geol Soc Am Bull 97:1037–1053

Ramsay JG, Graham RH (1970) Strain variations in shear belts. Can J Earth Sci 7:786–813

Ratschbacher L, Frisch W, Neubauer F, Schmid SM, Neugebauer J (1989) Extension in compressional orogenic belts. Geology 17:404–407

Ricou L-E (1994) Tethys reconstructed. Plates, blocks and their boundaries since 260 My from central America to Southeastern Asia. Geodin Acta 7:169–218

Ricou L-E, Burg J-P, Godfriaux I, Ivanov Z (1998) Rhodope and Vardar: the metamorphic and the olistostromic paired belts related to the cretaceous subduction under Europe. Geodin Acta 11:285–309

Robertson AHF, Dixon JE (1984) Introduction: aspects of the geological evolution of the eastern Mediterranean. In: Dixon JE, Robertson AHF (eds) The geological evolution of the eastern Mediterranean. Geol Soc Lond Sp Publ 17:1–74

Robertson AHF, Dixon JE, Brown S, Collins A, Morris A, Pickett E, Sharp I, Ustaömer T (1996) Alternative tectonic models for the late Palaeozoic-early tertiary development of tethys in the eastern Mediterranean region. In: Morris A, Tarling DH (eds) Paleomagnetism and tectonics of the Mediterranean region. Geol Soc Lond Sp Publ 105:239–263

Schmid S, Casey M (1986) Complete fabric analysis of some commonly observed quartz c-axis patterns. In: Mineral and rock deformation: laboratory studies—the paterson volume. AGU Monogr 36:263–286

Selverstone J (1988) Evidence for east-west crustal extension in the eastern Alps: implications for the unroofing history of the Tauern window. Tectonics 7:87–105

Schermer ER (1993) Geometry and kinematics of continental basement deformation during the Alpine orogeny, Mount Olympos region, Greece. J Struct Geol 15:571–591

Sokoutis D, Brun J-P, Van Den Driessche J, Pavlides S (1993) A major Oligo-Miocene detachment in southern Rhodope controlling north Aegean extension. J Geol Soc Lond 150:243–246

Soldatos T, Christofides G (1986) Rb-Sr geochronology and origin of the Elatia Pluton, central Rhodope, north Greece. Geol Balcanica 16:15–23

Teyssier C, Whitney D (2002) Gneiss domes and orogeny. Geology 30:1139–1142

von Braun E (1993) The Rhodope question viewed from eastern Greece. Z dt Geol Ges 144:406–418

Wallis SR, Platt JP, Knott SD (1993) Recognition of synconvergence extension in accretionary wedges with examples from the Calabrian arc and the eastern Alps. Am J Sci 293:463–495

Watterson J (1968) Homogeneous deformation of the gneisses of Vesterland, southwest Greenland. Medd Groenland 175:1–78

Wawrzenitz N, Mposkos E (1997) First evidence for lower cretaceous HP/HT-metamorphism in the eastern Rhodope, north Aegean region, north-east Greece. Eur J Miner 9:659–664

Wawrzenitz N, Krohe A (1998) Exhumation and doming of the thasos metamorphic core complex (S Rhodope, Greece): structural and geochronological constraints. Tectonophysics 285:301–332

Wenk HR (1994) Preferred orientation patterns in deformed quartzites. In: Ribbe PH (ed) Silica: physical behavior, geochemistry and materials applications. Rev Miner 29:177–208

Wernicke B (1981) Low-angle normal faults in the basin and range province: nappe tectonics in an extending orogen. Nature 291:645–648

Wernicke B, Burchfiel BC (1982) Modes of extensional tectonics. J Struct Geol 4:105–115

Yanev Y, Bardintzeff J-M (1997) Petrology, volcanology and matallogeny of palaeogene collision-related volcanism of the eastern Rhodopes (Bulgaria). Terra Nova 9:1–8